

**Amiodarone Irreversibly Impairs the Function of hERG Potassium  
Channels**

By

Illia Gelman

A thesis submitted to the Department of Biomedical and Molecular Sciences

In conformity with the requirements for

the degree of Master of Science

Queen's University

Kingston, Ontario, Canada

August, 2025

Copyright © Illia Gelman, 2025

## Abstract

Amiodarone (AMIO) is a class III antiarrhythmic drug (AAD) that blocks the human ether-a-go-go-related (hERG) channel which conducts the rapidly activating delayed rectifier potassium current,  $I_{Kr}$ . While effective in the treatment of certain arrhythmias, like other class III AADs, AMIO presents a significant risk of inducing long QT syndrome (LQTS). The present study investigates the inhibitory effects of AMIO on hERG channels heterologously expressed in HEK293 as well as rat cardiomyocyte-derived H9c2 cells. Acute application of AMIO or desethylamiodarone (DEA) inhibited the hERG current ( $I_{hERG}$ ) in a concentration-dependent manner with an  $IC_{50}$  of 0.22  $\mu$ M or 0.95  $\mu$ M, respectively. Surprisingly, upon washout of the compounds and recording  $I_{hERG}$  in a drug-free bath solution, no current recovery was observed from either the AMIO- or DEA-induced inhibition. Furthermore, after overnight (16 h) treatment of cells with the drugs and recordings were made in the absence of drugs, AMIO or DEA treatment resulted in a concentration-dependent  $I_{hERG}$  reduction with an  $EC_{50}$  of 0.32  $\mu$ M or 0.85  $\mu$ M, respectively. Western blot analysis of hERG channel expression revealed that although AMIO overnight treatment did not affect hERG protein expression, it accelerated the degradation rate of mature hERG protein when AMIO-treated cells were further cultured in the absence of the drug. This suggests that the fundamental properties of these channels, such as membrane stability and function, are affected by AMIO treatment. Our results indicate that both AMIO and DEA irrecoverably impair hERG function, with  $I_{hERG}$  recovery is dependent on the forward trafficking of newly made channels, which takes place in hours. Thus, it would be imperative to monitor electrophysiology of the heart in patients discontinuing AMIO therapy due to LQTS.

## **Co-Authorship**

This thesis represents original work by Illia Gelman. Shetuan Zhang conceptualized the project and guided the experimental design. Shetuan Zhang and Illia Gelman designed experiments with the help from Wentao Li and Jun Guo. Jun Guo performed cell culture and cDNA transfections. Jun Guo and Illia Gelman administered the overnight-applied treatments. Neelakshi Sharma, Nicole Tomei, and Illia Gelman collected all of the Western blot data. Illia Gelman analyzed all of the Western blot results. Electrophysiology results were collected and analyzed by Wentao Li, Jun Guo, and Illia Gelman. Generally, Illia Gelman collected at least 50% of all experimental data. Shetuan Zhang, Wentao Li, and Illia Gelman created the figures. Illia Gelman organized the data and independently wrote the thesis.

## Acknowledgements

They say science stands on the shoulders of giants – to me this means that science has been built on decades of previous work as much as it highlights how important one's support system is. I am extremely grateful and lucky to have had the opportunity to complete my Master's research project working alongside an amazingly supportive team. All of the guidance and support I have received – both professional and otherwise – have made for a formative two years at the Zhang lab. With that, I would like to first thank my supervisor, Dr. Shetuan Zhang, for being a demanding, yet understanding mentor. You have provided me with so many opportunities to grow professionally and personally, and I am confident this experience will contribute greatly to shaping my future. I would also like to thank Wentao Li and Jun Guo for their technical support and patience when teaching me new laboratory techniques or troubleshooting various assays. Without your knowledge and willingness to help, I would not have been able to complete my project. Finally, I would like to thank Tonghua Yang for always being there for me and the other students, be it with a word of advice or a helping hand. I would be remiss if I didn't mention the students, past and present, that have also contributed greatly to this Master's being an extremely enjoyable experience. I would like to thank Reese Cherry, Angelia Pan, Neelakshi Sharma, and Nicole Tomei for their help with my project. I would also like to thank Ananya Chakraborty and James (Duncan) Cornwell for their mentorship. Finally, I want to extend another bonus thank-you to all of the members of the Zhang lab for making these past two years feel like I had never left home.

I am also ever so grateful for the thorough groundwork of electrophysiological knowledge laid by Dr. Neil Magoski and Dr. Alastair Ferguson. Having taken the Ion Channels course has greatly expanded my understanding of electrophysiology and has reinforced my appreciation for research in the field. I would also like to separately thank my thesis advisory committee members,

Dr. Neil Magoski and Dr. Christopher Ward, for their continued help and support throughout my project.

Next, I would like to extend a thank-you to all of the amazing friends I have made on this and other floors of our beloved laboratory building. I would like to thank Emily Robichaud and Hayley Albert of the Magoski lab, Julia Vassalakis of the Postovit lab, and Angela Loureiro of the Maurice lab for all the great times both in and out of the lab. Having you around has made the past two years fly by like a breeze.

Last but not least, I would like to express a heartfelt thank-you to my immediate family – my mother, my father, and my younger brother. While you were not able to stay near physically, you have always been there for me in spirit (and on FaceTime) to offer a word of advice. I would not be where I am today, if it were not for my family.

## Table of Contents

<b>Abstract</b> .....	ii
<b>Co-Authorship</b> .....	iii
<b>Acknowledgements</b> .....	iv
<b>List of Figures</b> .....	vii
<b>List of Abbreviations</b> .....	viii
<b>Chapter 1 – Introduction and Literature Review</b> .....	1
1.1 The Cardiac Action Potential .....	1
1.2 The hERG K <sup>+</sup> channel .....	4
1.2.1 Structure and Function .....	4
1.2.2 Gating and Kinetics.....	8
1.2.3 Drug Block and Long QT Syndrome .....	10
1.3 Amiodarone.....	13
1.4 Hypothesis and Objectives.....	15
<b>Chapter 2 – Materials and Methods</b> .....	17
2.1 Cell Culture and Molecular Biology .....	17
2.2 Western Blot Analysis .....	18
2.3 Patch Clamp Electrophysiology.....	20
2.4 Drugs and Treatments .....	22
2.5 Statistical Analysis .....	23
<b>Chapter 3 – Results</b> .....	24
3.1 Chronic AMIO inhibits I <sub>hERG</sub> but does not affect mature hERG channel expression .....	24
3.2 AMIO irreversibly inhibits I <sub>hERG</sub> .....	28
3.3 The effects of AMIO on mutant hERG channels .....	31
3.4 I <sub>hERG</sub> recovery in AMIO-treated cells is dependent on newly made channels .....	35
3.5 AMIO modulates the rate of mature hERG channel degradation .....	39
3.6 DEA displays a similar interaction with hERG as AMIO.....	39
3.7 hERG channels heterologously expressed in cardiomyocyte-derived H9c2 cells are similarly blocked by AMIO and DEA .....	44
<b>Chapter 4 – Discussion</b> .....	46
<b>Future directions</b> .....	50
<b>References</b> .....	52

## List of Figures

<b>Figure 1. The ventricular action potential and corresponding ion channel currents.</b> .....	2
<b>Figure 2. hERG channel tetramer structure.</b> .....	5
<b>Figure 3. Structural differences between hERG1a and hERG1b isoforms.</b> .....	7
<b>Figure 4. hERG gating and kinetics.</b> .....	9
<b>Figure 5. Delayed repolarization and LQTS associated with <math>I_{hERG}</math> block.</b> .....	12
<b>Figure 6. Overnight AMIO application decreases <math>I_{hERG}</math> recorded in hERG-HEK cells in drug-free conditions.</b> .....	25
<b>Figure 7. Mature hERG expression in hERG-HEK cells remained unaffected following overnight culture with AMIO.</b> .....	27
<b>Figure 8. AMIO irrecoverably inhibits <math>I_{hERG}</math>.</b> .....	29
<b>Figure 9. AMIO-induced block of <math>I_{hERG}</math> is frequency- and use-dependent.</b> .....	32
<b>Figure 10. AMIO shares binding sites with other class III agents.</b> .....	34
<b>Figure 11. Recovery of <math>I_{hERG}</math> from AMIO treated cells relies on newly trafficked mature channels.</b> .....	36
<b>Figure 12. Effects of AMIO on the degradation of mature hERG proteins.</b> .....	40
<b>Figure 13. DEA, the major metabolite of AMIO, also irrecoverably inhibits <math>I_{hERG}</math>.</b> .....	43
<b>Figure 14. Acute effects of AMIO and DEA on the currents of hERG channels heterologously expressed in H9c2 cells.</b> .....	45

## List of Abbreviations

AP	action potential
AAD	antiarrhythmic drug
APD	action potential duration
AMIO	amiodarone
Baf	bafilomycin
BFA	brefeldin A
cAMP	cyclic adenosine monophosphate
CM	cardiomyocyte
CNBD	cyclic-nucleotide binding domain
CTL	control
D-PBS	Dulbecco's phosphate-buffered saline
DC	detergent-compatible
ddH <sub>2</sub> O	double-distilled water
DEA	N-desethylamiodarone
EAD	early afterdepolarization
ECG	electrocardiogram
HCN	hyperpolarization-activated cyclic nucleotide-gated (channels)
hERG	human ether-a-go-go-related gene
I <sub>Ca</sub>	L-type Ca <sup>2+</sup> current
I <sub>f</sub>	funny current
I <sub>K1</sub>	inwardly-rectifying K <sup>+</sup> current
I <sub>Kr</sub>	rapid delayed rectifier current

$I_{Ks}$	slow delayed rectifier current
$I_{Na}$	$Na^+$ current
$I_{to}$	transient outward $K^+$ current
LQTS	long QT syndrome
PAS	Per-Arnt-Sim domain
PK	proteinase K
PMSF	phenylmethylsulfonyl fluoride
PVDF	polyvinylidene difluoride
SAN	sinoatrial node
SDS	sodium dodecyl sulfate
SF	selectivity filter
TBST	tris-buffered saline with Tween 20
TdP	Torsades de Pointes arrhythmia
VSD	voltage sensing domain
WT	wild-type

# Chapter 1 – Introduction and Literature Review

## 1.1 The Cardiac Action Potential

Cardiac rhythm is maintained by the fine balance of the in- and outflow of  $\text{Na}^+$ ,  $\text{Ca}^{2+}$ , and  $\text{K}^+$  ions through ligand- and voltage-gated ion channels. The sequence and magnitude of inward  $\text{Na}^+$  and  $\text{Ca}^{2+}$  currents and outward  $\text{K}^+$  currents are what define the shape of the cardiac action potential (AP). These APs originate from pacemaker cells located in the sinoatrial node (SAN) and propagate throughout the myocardium via the cardiac conduction system, triggering rhythmic and synchronized contractions (Amin et al., 2010). Hyperpolarization-activated cyclic nucleotide-gated (HCN) channels grant SAN cardiomyocytes (CM) their autorhythmic property by conducting a net depolarizing current at hyperpolarized membrane potentials and driving the membrane to the threshold potential (Baruscotti et al., 2005). HCN channels are permeable to both  $\text{Na}^+$  and  $\text{K}^+$  ions, are activated by hyperpolarization and cyclic adenosine monophosphate (cAMP), and conduct what is referred to as the funny current ( $I_f$ ) (Baruscotti et al., 2005). While pacemaker cells do not depend on external stimulation to generate spontaneous APs, the SAN is heavily innervated by both sympathetic and parasympathetic nerve endings that modulate the rate of pacemaker cell firing (Behar et al., 2016).

As the membrane ion channel content varies between types of CMs, so do the AP morphologies that propagate through each respective portion of the heart. These are broken down into pacemaker, atrial, and ventricular APs that can be recognized by their distinct amplitude and duration (Amin et al., 2010). This thesis will focus on the ventricular AP as the channel being investigated is predominantly expressed in the ventricles. The ventricular AP consists of 5 phases, with the CM membrane resting between -90 mV and -80 mV during phase 4 (Fig. 1)

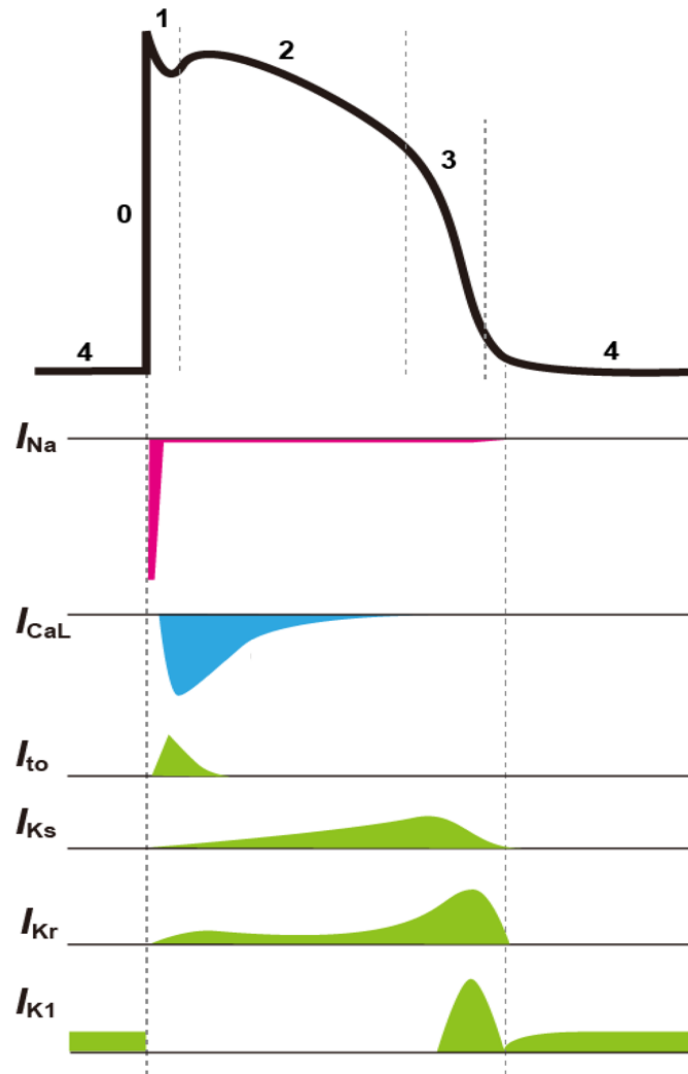


**Figure 1. The ventricular action potential and corresponding ion channel currents.**

Schematic representation of the AP waveform of non-autorhythmic ventricular cardiomyocytes with the ionic currents involved presented below. The resting membrane potential throughout phase 4 is maintained primarily by  $I_{K1}$  through  $K_{ir}2.1$  channels. Upon an external depolarizing stimulus, activation of the  $Na_v1.5$ -mediated  $I_{Na}$  creates the upstroke of the AP observed during phase 0. Slight repolarization of the membrane in phase 1 occurs due to the rapid activation of  $I_{to}$ . The membrane potential is stabilized during the plateau phase, or phase 2, as the result of the L-type  $Ca_v1.2$  channels activating and passing inward  $I_{Ca-L}$ . Finally, the action potential is terminated during phase 3, or the repolarization phase, where outward  $K^+$  conductance, represented by  $I_{Kr}$ ,  $I_{Ks}$ , and  $I_{K1}$ , returns the membrane to its resting potential. Figure modified from Tsumoto and Kurata (2022).

(Amin et al., 2010). The resting membrane potential is maintained by inwardly-rectifying  $K^+$  channels of the  $K_{ir2.x}$  family that conduct the inwardly-rectifying  $K^+$  current ( $I_{K1}$ ) (Dhamoon and Jalife, 2005). These channels activate at hyperpolarized membrane potentials more negative than the reversal potential of  $K^+$ , resulting in an inward  $K^+$  conductance (Dhamoon and Jalife, 2005). Phase 0 begins when a strong external depolarizing stimulus results in the activation of  $Nav1.5$  channels, creating a large inward  $Na^+$  current ( $I_{Na}$ ) and driving rapid membrane depolarization to initiate the AP (DeMarco and Clancy, 2016). This leads to a subsequent activation of the transient outward  $K^+$  current ( $I_{to}$ ) in phase 1 conducted by  $Kv4.3$  channels, which repolarizes the membrane slightly and can be observed on the AP waveform as a notch immediately following the upstroke (Patel and Campbell, 2005; Tristani-Firouzi et al., 2001). During phase 2, the transient repolarization driven by  $I_{to}$  is offset by an inward L-type  $Ca^{2+}$  current ( $I_{Ca-L}$ ), conducted by  $Ca_v1.2$  channels (Grant, 2009). In addition, the slow activation of the rapid and slow delayed rectifier currents ( $I_{Kr}$  and  $I_{Ks}$ , respectively) briefly stabilizes the membrane potential resulting in a characteristic plateau (Tristani-Firouzi et al., 2001). This allows enough time for calcium-induced calcium release from the sarcoplasmic reticulum and the subsequent contraction of the ventricular CMs (Grant, 2009; Sobie and Ramay, 2009). During phase 3 of the ventricular AP,  $I_{Kr}$  and  $I_{Ks}$  finally reach their maximum magnitudes and drive the initial repolarization of the CM membrane (Tristani-Firouzi et al., 2001). After the initial slow activation and rapid inactivation, the negative shift in the membrane potential triggers the recovery from inactivation of a large outward  $I_{Kr}$  conductance passed by the human ether-a-go-go-related gene (hERG)  $K^+$  channel (Sanguinetti et al., 1995; Tristani-Firouzi et al., 2001). Assisted by the resurgence in the outward  $I_{K1}$  during late phase 3, this terminates the ventricular AP, returning the membrane to its resting potential (Tristani-Firouzi et al., 2001). Therefore,  $I_{Kr}$  represents an essential component in ventricular

repolarization, thus also modulating the action potential duration (APD) in ventricular CMs (Sanguinetti et al., 1995).

## 1.2 The hERG K<sup>+</sup> channel

### 1.2.1 Structure and Function

The individual pore-forming  $\alpha$ -subunits of the hERG channel, also known as Kv11.1, are encoded by the gene of the same name, *hERG*, with homo-tetrameric channels passing a current that closely resembles the native  $I_{Kr}$  (Sale et al., 2008). An assembled hERG channel consists of 4 subunits. Each subunit is comprised of several domains (Fig. 2A). Starting at the N-terminus, the first 135 of 390 amino acid residues comprise the Per-Arnt-Sim (PAS) domain that has been found to play a role in the modulation of hERG deactivation kinetics (Fig. 2B) (Morais Cabral et al., 1998). Morais Cabral et al. (1998) have shown that the deletion of the PAS domain results in a deactivation time-constant reduction of 5-10 times. Moreover, mutagenesis studies have shown that breaking or removing the amphipathic helix at residues 1-26 (NT1-26) dramatically accelerates the slow deactivation kinetics observed in heterologously expressed hERG channels, likely acting as a regulatory portion of the PAS domain (Gustina and Trudeau, 2012). This effect was found to rely on the interaction between the positively-charged residues within the PAS and the negatively-charged residues of the cyclic-nucleotide binding domain (CNBD) located on the C-terminal side (Fig. 2B) (Muskett et al., 2011; Ng et al., 2011). More specifically, the positively-charged face of the NT1-26 interacts with negatively-charged pockets located within the CNBD, as shown by experiments involving charge reversal mutagenesis (Muskett et al., 2011). Besides modulating the channel deactivation kinetics, the PAS and CNBD domains are also thought to be involved in the maturation and forward trafficking to the membrane

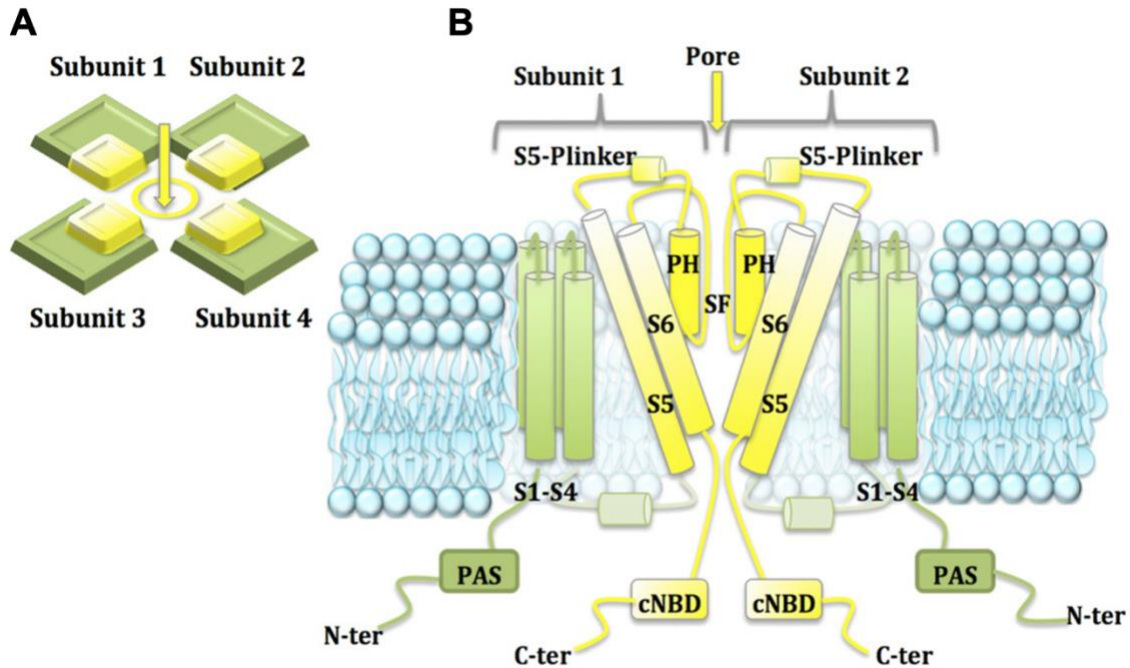


**Figure 2. hERG channel tetramer structure.**

A. Schematic representation of an assembled hERG channel tetramer with the VSD (green) pointed outwards and the pore-forming S5-S6 subunits (yellow) directed inwards to create the ion conduction pathway (yellow circle). B. Schematic representation of subunit organization in a cross-sectional view of the hERG channel (only 2 of the 4 subunits shown). The N-terminus, which contains the PAS, is located intracellularly. The VSD is formed by transmembrane domains S1-S4, while the pore domain contains domains S5-S6. The pore is formed by the S5-S6 linker, which contains the pore helix (PH) and the selectivity filter (SF). The C-terminus, containing the CNBD, is also located intracellularly. Figure modified from Kalyanamoorthy and Barakat (2018).

of newly made hERG channels. Mutations in these domains have been described as trafficking deficient, with hERG protein failing to undergo maturation and becoming subject to proteasomal degradation (Akhavan et al., 2003; Foo et al., 2019). Finally, the hERG channel contains 6 transmembrane domains, labeled S1 through S6, with domains S1-S4 acting as the voltage sensing domain (VSD) and S5-S6 as the pore domain (Fig. 2B) (Perry et al., 2010). When hERG is assembled and functional on the membrane surface, S5-S6 linkers of the 4 channel subunits come together to form the ion conduction pathway (Perry et al., 2010; Zünkler, 2006). The hERG S5-S6 linker is unusually long and contains a pore helix (PH) that is thought to electrostatically link the VSD to the selectivity filter (SF), modulating inactivation gating (Butler et al., 2019). Lining the pore cavity is the SF. In contrast to Gly-Tyr-Gly observed in most other K<sup>+</sup> channels, hERG contains a Gly-Phe-Gly motif believed to contribute to its fast inactivation kinetics (Perry et al., 2010; Zünkler, 2006).

In native ventricular tissue, hERG is expressed as two isoforms, hERG1a and hERG1b (Fig 3A, B). The N-terminus of hERG1b is considerably shorter than that of hERG1a, containing a unique 58 amino acid-long sequence and thus lacking the PAS domain of the 1a isoform (Fig. 3A, B). Starting at position 37 in hERG1b and 377 in hERG1a, the remainder of the amino acid sequences are identical (Johnson et al., 2022). While homotetrameric hERG1b channels display smaller currents and much faster deactivation; accelerated activation, deactivation, and recovery from inactivation have been observed in heterotetrameric hERG1a/1b channels (Jones et al., 2014; McNally et al., 2017). Kinetics of the currents passed by heterotetrameric hERG channels more closely resemble native I<sub>Kr</sub>, suggesting that both contribute to the native current (Jones et al., 2014). In addition, heterotetrameric channels have been found to display altered drug sensitivity compared to homomeric hERG1a channels. For example, fluoxetine displayed higher blocking

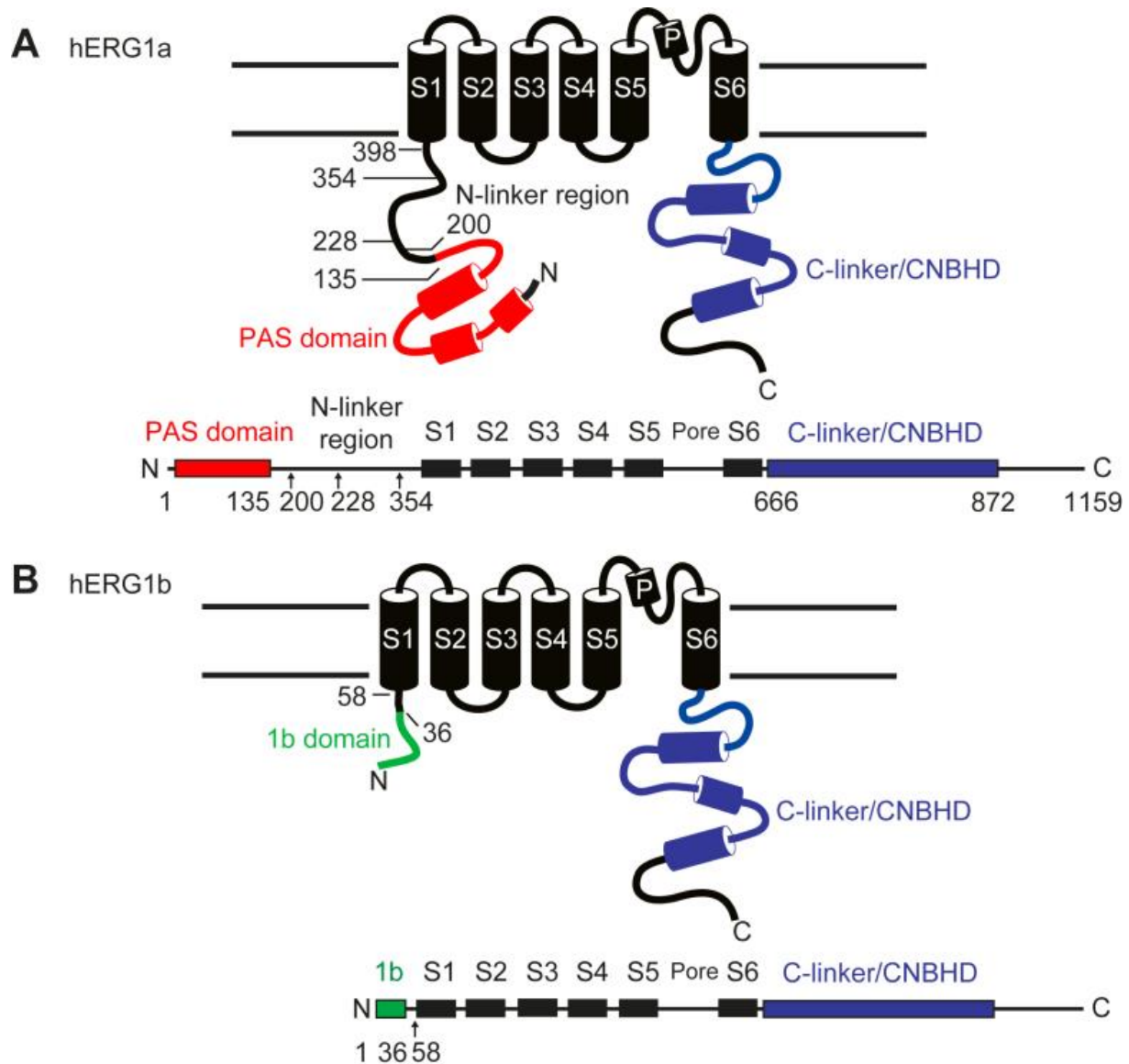


**Figure 3. Structural differences between hERG1a and hERG1b isoforms.**

A. Schematic representation of the hERG1a isoform within the membrane (upper panel) as well as in linear view (lower panel). The N-terminus contains the PAS domain and a long N-linker region; B. Schematic representation of the hERG1b isoform within the membrane (upper panel) as well as in linear view (lower panel). The N-terminus is truncated, containing a unique amino acid sequence at positions 1-36. Beyond the 37th residue of hERG1b, it is identical to the 1a isoform starting at position 377. Figure adapted from Johnson *et al.* (2022).

potency in the former, while E-4031 more potently blocked the latter (Abi-Gerges et al., 2011). In this thesis, the term “hERG” will be used to describe homotetrameric hERG1a channels and their conductance, as this form of the channel is studied in most literature.

### 1.2.2 Gating and Kinetics

hERG channels display unique gating kinetics when compared to other cardiac  $K^+$  channels. Fundamentally, the hERG channel can exist in 3 states – closed, open, and inactivated – with current only passed in the open state. Although hERG passes the rapidly activating delayed rectifier current, transition between the closed and open states is relatively slow when compared to other voltage-gated ion channels (Perry et al., 2015). The rapid kinetics of hERG inactivation, recognized as atypical C-type inactivation, and recovery therefrom remain largely unexplained. It is hypothesized, however, that they result from a rapid and reversible rearrangement and collapse of the SF as the result of  $K^+$  efflux during initial channel opening (Shi et al., 2020). In addition, inactivation of hERG channels is strongly voltage-dependent, increasing with more depolarized membrane potentials. This gives rise to the phenomenon of inward rectification, whereby the increased rate of inactivation at membrane potentials more positive than the reversal potential limits  $K^+$  efflux (Kiehn et al., 1999a; Smith et al., 1996). On the other hand, at potentials negative to the reversal potential, inactivation is minimal, allowing for an increased conductance (Smith et al., 1996). In its closed state, the hERG pore cavity is occluded by the activation gate which is electrostatically coupled to the VSD through the S4-S5 linker (Fig. 4A). This allows for voltage-dependent channel opening and stabilizes the closed state of the channel (Ferrer et al., 2006; Shi et al., 2020).

Taken together, the gating kinetics of hERG channels support its role as a physiologically important repolarizing current. Upon initial depolarization of the membrane, such as during phase

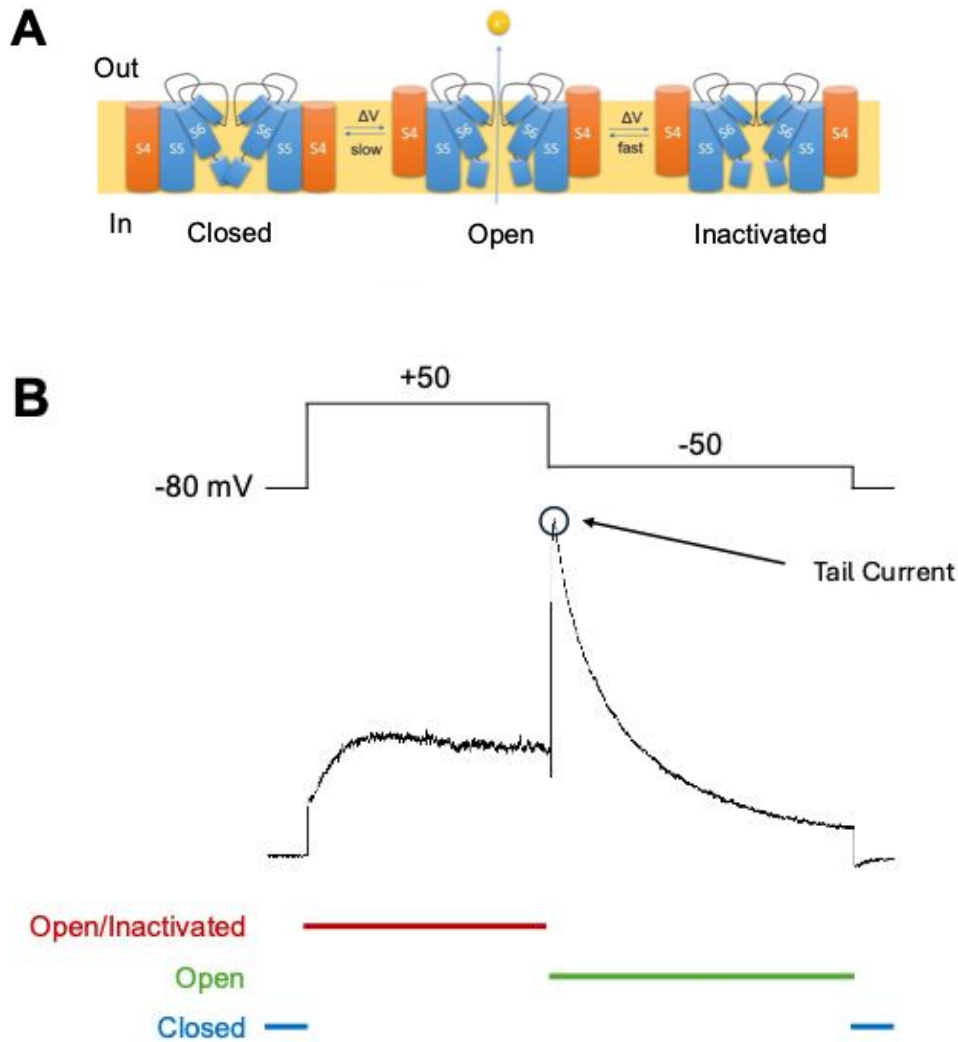


**Figure 4. hERG gating and kinetics.**

A. Schematic representation of the 3 states of the hERG channel. hERG can exist in 3 possible states – closed, open, and inactivated. Transition between the closed and open states is slow, while that between open and inactivated states is extremely rapid. In the closed state the activation gate fully occludes the pore cavity. Inactivation occurs through occlusion of the pore due to a rearrangement of the SF upon initial channel opening. Panel adapted from Shan *et al.* (2022). B. Representative  $I_{hERG}$  trace with a corresponding voltage protocol. Upon initial membrane depolarization (+50 mV), channels open slowly and inactivate rapidly. Repolarization (-50 mV) of the membrane triggers a fast recovery from inactivation, producing a characteristic surge, referred to as the tail current. Return to holding potential (-80 mV) forces the channels to close, stopping the  $I_{hERG}$  conductance.

0 of the ventricular AP, the channels slowly transition from a closed to an open state but inactivate rapidly. As the membrane begins to repolarize, recovery from inactivation occurs extremely rapidly ( $\tau$  in 1 ms), producing a large outward conductance with a sharp peak that is termed the “tail current” (Fig. 4B) (Vandenberg et al., 2006). In the heart, this produces the large repolarizing current necessary to terminate the AP (Sanguinetti et al., 1995; Tristani-Firouzi et al., 2001).

The structure of the hERG channel is directly linked to its kinetics, with mutations in crucial locations producing drastic changes in its gating mechanisms. As mentioned before, the N- and C-termini play a role in the slow deactivation kinetics of hERG. N-terminal deletion results in a positive shift in activation voltage as well as accelerated channel deactivation (Gustina and Trudeau, 2012). Similarly, C-terminus-truncated mutants, lacking the CNBD, display accelerated deactivation gating and a positive shift in activation voltage. However, activation kinetics of CNBD-deleted mutants were also found significantly accelerated, indicating a possible role for the CNBD in activation gating (Gustina and Trudeau, 2011). Mutations in the S5-S6 pore linker, such as S620T and S631A, have been noted to attenuate C-type inactivation, either by preventing full constriction of the SF or by positively shifting the voltage-dependence of inactivation and abolishing rectification, respectively (Li et al., 2021; Zou et al., 1998).

### **1.2.3 Drug Block and Long QT Syndrome**

Certain features of the hERG channel confer its extremely high propensity for drug-channel interactions. Namely, the S6 helix contains two aromatic amino acid residues – Tyr at position 652 (Y652) and Phe at position 656 (F656) – that project into the pore cavity and are able to bind drugs in the ion conduction pathway, thus blocking ion flux. Mutations in these residues (Y652A, F656V) drastically reduce binding potency for such high-affinity channel blockers as MK-499, E-4031, and dofetilide (Lees-Miller et al., 2000; Milnes et al., 2003; Mitcheson et al., 2000a). About

60% of drug candidates across all drug classes display an affinity for interactions with hERG (Vandenberg et al., 2017). The danger stems from the APD prolongation that occurs due to a drug-hERG interaction, whereby drug binding within the pore blocks hERG current ( $I_{hERG}$ ) and leads to delayed cardiac repolarization, an excess of which carries significant arrhythmogenic risk (Vandenberg et al., 2017). This is because that prolongation of the APD beyond a certain duration can allow enough time for L-type  $Ca^{2+}$  channels to recover from inactivation and produce a premature membrane depolarization, also known as an early afterdepolarization (EAD) (Fig. 5A) (Tsuji et al., 2024).

On an electrocardiogram (ECG) tracing, APD prolongation is reflected as an extended QT interval, which represents ventricular depolarization (QRS complex) and repolarization (T wave) (Fig. 5B) (Kallergis et al., 2012). Excessive prolongation of the QT interval is referred to as long QT syndrome (LQTS) and carries a significant risk of fatal arrhythmia (Fig. 5B) (Kallergis et al., 2012). It can occur either due to a loss-of-function mutation in the hERG protein or as a result of a drug interaction with the channel, leading to its blockade (Foo et al., 2016). When EADs occur, the depolarization can spread to surrounding tissue, causing aberrant firing in CMs and leading to polymorphic ventricular tachyarrhythmia, also known as Torsades de Pointes arrhythmia (TdP) (Fig. 5B). This arrhythmia can be self-limiting; however, it carries a high risk of degenerating into life-threatening ventricular fibrillation with reported 10.7% in-hospital and 25% 1-year mortality rates (Mantri et al., 2022; Wolfes et al., 2024). Management options for TdP are limited and include intravenous magnesium sulfate administration and electrolyte repletion with a focus on  $K^+$  (Bailie et al., 1988; Drew et al., 2010; Gupta et al., 2007; Kaseda et al., 1989; White et al., 1999). If such an episode is suspected to have resulted from a drug-hERG interaction, discontinuation of treatment with the offending compound is recommended (Drew et al., 2010; Gupta et al., 2007).

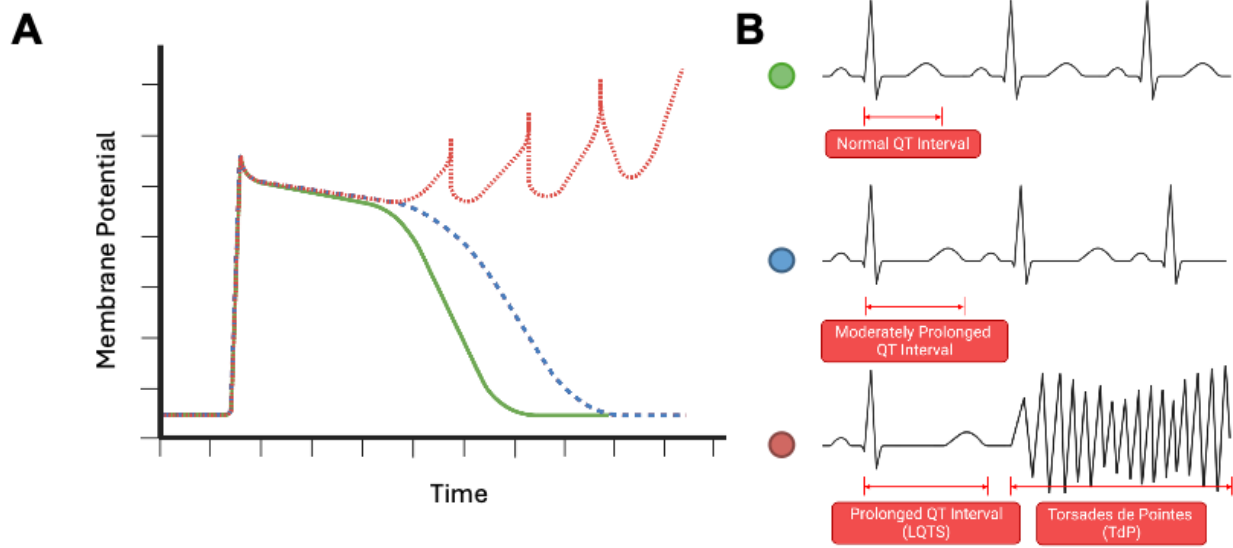


**Figure 5. Delayed repolarization and LQTS associated with  $I_{hERG}$  block.**

A. Schematic representation of ventricular AP morphology in the normal condition (green line), with slightly delayed repolarization (blue dotted line), and with an early afterdepolarization (red dotted line). APD prolongation represents significant risk of ectopic AP formation and thus ventricular arrhythmia. Panel made using biorender.com B. Schematic ECG strip (dot colors next to trace correspond to schematic AP tracings in A) highlighting the QT interval in the normal condition (upper panel), with slight QT prolongation (middle panel), and with significant QT interval prolongation (LQTS) escalating into polymorphic ventricular tachyarrhythmia, also known as Torsades de Pointes arrhythmia (lower panel). Panel modified from Gelman *et al.* (2024).

### 1.3 Amiodarone

Amiodarone (AMIO) is a benzofuran-based antiarrhythmic drug (AAD) that is commonly used in the clinic for the treatment of ventricular fibrillation and, more recently, atrial fibrillation (Istratoaie et al., 2021; Milberg et al., 2004; Van Herendael and Dorian, 2010). Its main effect in the heart corresponds to the classical mechanism of action of class III AADs – hERG blockade by binding to residues Y652 and F656 in the ion conduction pathway. However, it also binds to and blocks cardiac  $\text{Na}^+$  and  $\text{Ca}^{2+}$  channels as well as possesses beta-blocking activity (Kodama et al., 1997; Mujovic et al., 2020; Ridley et al., 2004). This multiple-channel blocking activity is believed to confer its higher effectiveness in preventing arrhythmic episodes (Milberg et al., 2004). Particularly, midmyocardial M cells, unlike epicardial and endocardial cells, can sustain a larger APD prolongation in response to AAD application, leaving them refractory, and thus unable to fire, for longer periods than surrounding tissue (Sicouri and Antzelevitch, 1991). When an ectopic AP encounters this unidirectional block, it is redirected to the endocardium and then back towards the midmyocardium and the pericardium that are no longer refractive (Belardinelli et al., 2003). Therefore, AMIO acts to decrease the heterogeneity of APDs between neighboring CMs and equalizes their effective refractory periods, thus largely preventing re-entry (Drouin et al., 1998; Sicouri et al., 1997). Finally, AMIO can prevent EAD formation by inhibiting late  $I_{\text{Na}}$  and  $I_{\text{Ca,L}}$ , further limiting arrhythmogenic risk (Horvath et al., 2013; Horvath et al., 2015). Nonetheless, like other class III AADs, AMIO still carries a tangible risk of LQTS and TdP (Milberg et al., 2004).

AMIO is highly lipophilic, readily distributing into vascularized tissue out of the plasma (Freedman and Somberg, 1991; Latini et al., 1984). Its apparent volume of distribution was measured to range from 0.9 to 148 l/kg (Latini et al., 1984). After entering the circulation, either following intravenous or oral administration, AMIO is extensively metabolized in the liver

primarily by CYP450 3A enzymes (Freedman and Somberg, 1991; Shayeganpour et al., 2006). This step results in the production of its main active metabolite, N-desethylamiodarone (DEA), which is even more lipophilic than its parent compound and has also been noted to exhibit class III antiarrhythmic properties (Freedman and Somberg, 1991). When plasma AMIO and DEA concentrations were analyzed against their concentrations within the myocardium, partitioning coefficients of 35 and 91, respectively, indicated significantly higher tissue/plasma concentration ratios for both compounds (Freedman and Somberg, 1991). Hepatic metabolism represents the main elimination pathway for AMIO, with urinary excretion accounting for less than 1% of active compound removed (Latini et al., 1984). Finally, in the plasma, an overwhelmingly large proportion of the drug is in a protein-bound state, with measurements ranging from 96.3% to as high as 99.9% (Latini et al., 1984; Veronese et al., 1988).

The high lipophilicity of AMIO and its active metabolite are believed to play a role in the extremely slow elimination kinetics of the compound. Namely, the half-life of AMIO in the human body has been found to range from 1-3 months (Kannan et al., 1987; Marchiset et al., 1985). Moreover, therapeutic concentrations of the drug were observed to remain in the plasma for over a month following withdrawal of long-term therapy (Latini et al., 1984). Combined with minimal renal excretion, and thus insusceptibility to dialysis treatment, as well as extended effects of the active metabolite DEA, the persistence of AMIO within the body may be of concern if the therapy precipitates LQTS or TdP (Latini et al., 1984). However, whether the drug's prolonged effects depend solely on its pharmacokinetic profile remains poorly understood, as days-long recovery periods have been reported even after short-term intravenous infusions (Yonai et al., 2021).

## 1.4 Hypothesis and Objectives

. While AMIO has been clinically used to treat a wide range of arrhythmias for over 30 years, its channel-blocking properties remain largely underexplored (Van Herendael and Dorian, 2010). For example, while the acute effects of the drug on cardiac ion channels have been described, few studies to date have looked into the chronic effects of its administration (Kauthale et al., 2015; Kiehn et al., 1999b; McPate et al., 2008; Ridley et al., 2004; Zhang et al., 2016; Zhang et al., 2010). More specifically, chronic effects of AMIO on hERG channel function and expression have not been investigated. Thus, elucidating the mechanisms for chronic treatment with AMIO-induced potential inhibition of hERG function will provide invaluable insight into its potent antiarrhythmic action and potentially further explain its slow elimination profile. We hypothesized that AMIO may display a unique interaction with the hERG channel. Furthermore, the mechanism of action of its main active metabolite, DEA, also remains largely unelucidated. While it is known that DEA largely shares the ion channel blocking profile of its parent compound, except for its effects on  $I_{Ca-L}$ , little is known about its chronic effects on hERG (Ghovanloo et al., 2016; Wagner et al., 1990; Zhang et al., 2010). Considering the similar molecular structure and pharmacokinetic profiles of AMIO and DEA, we hypothesized that DEA would interact with the hERG channel in a manner similar to its parent compound.

To test these hypotheses, we investigated the effects of chronic (overnight) treatment with AMIO and DEA on  $I_{hERG}$  and hERG protein expression. These experiments were performed in HEK293 cells stably expressing the wild-type (WT) hERG1a subunit using Western blot analysis and whole-cell patch-clamp recordings. Furthermore, we characterized the effects of chronic AMIO and DEA applications on hERG channels heterologously expressed in a cardiomyocyte-derived H9c2 cell line. Our results revealed a unique and previously unknown mode of drug-

channel interaction. We found AMIO irreversibly impaired hERG channel function and recovery of hERG function depended entirely on newly made channels. These findings would not only interest researchers but also healthcare professionals as they add a novel explanation for the long-lasting effects of AMIO after the termination of its therapy.

## Chapter 2 – Materials and Methods

### 2.1 Cell Culture and Molecular Biology

WT hERG cDNA was kindly provided by Dr. Gail A. Robertson (University of Wisconsin, Madison, WI). Mutant hERG cDNA with N-terminal deletion ( $\Delta$ 2-354), C-terminal truncation at position 1073 ( $\Delta$ C-1073), and point mutations in the pore region (S620T, S631A) or common drug-binding sites (Y652A, F656V) were constructed by PCR and verified by DNA sequencing as previously described; these also contained a geneticin/G418 resistance construct (Guo et al., 2007; Massaelli et al., 2010). All of the above were contained in a pcDNA3 vector. Transient transfection of mutant cDNA into HEK293 cells was performed using 2  $\mu$ g/ml hERG cDNA alongside 0.5  $\mu$ g/ml green fluorescent protein (GFP) cDNA (pIRES2-EGFP (enhance GFP); Takara Bio USA, San Jose, CA) in the presence of Lipofectamine 2000 (Thermo-Fisher Scientific, Waltham, MA). Cells were cultured in minimum essential medium (MEM, Gibco) supplemented with 10% fetal bovine serum (FBS), nonessential amino acids, and 1 mM sodium pyruvate (Thermo-Fisher Scientific, Waltham, MA). Following transfection, G418 was also added to the culture medium for selection (1 mg/ml) and maintenance (0.4 mg/ml) of transfected cells. An HEK293 cell line stably expressing WT hERG (hERG-HEK cells) was obtained from Dr. Craig T. January (University of Wisconsin, Madison, WI).

The H9c2 cell line was obtained from the American Type Culture Collection (Manassas, VA). For transient transfection of WT hERG cDNA, the same protocol was used as described above for HEK293 cells, except Lipofectamine 3000 was used (Thermo-Fisher Scientific, Waltham, MA). H9c2 cells were culture in Dulbecco's modified eagle medium (DMEM, Gibco) containing 10% FBS.

All cells were cultured at 37°C and 5% CO<sub>2</sub> and passaged every 48 hours so as to not exceed 80-90% confluency. For passaging, the cells were first washed with Ca<sup>2+</sup>-free Dulbecco's phosphate-buffered saline (D-PBS), treated with 5% trypsin in EDTA for 1-2 min until the cells start to visibly detach from the bottom of a culture dish, and replated with MEM or DMEM, as indicated for each cell line.

## 2.2 Western Blot Analysis

After their respective treatments, hERG-HEK cells were washed with ice-cold PBS and detached from the culture dish using a rubber cell scraper. The samples were then centrifugated at 1000 g for 4 min to pellet the cells, and the supernatant was aspirated and discarded. The cell pellets were resuspended in 70 µl of radioimmunoprecipitation assay lysis buffer containing 5% 20× broad spectrum cOmplete protease inhibitor cocktail (Roche Diagnostics, Mannheim, Germany) and 1 mM phenylmethylsulfonyl fluoride (PMSF). The lysis buffer itself contained 50 mM Tris-HCl, 150 mM NaCl, 1 mM EDTA, 5 µg/ml aprotinin, 5 mg/ml leupeptin, 1% Triton X-100, 1% sodium deoxycholate, and 0.1% sodium dodecyl sulfate (SDS) and was stored at 4°C. The samples were further processed using an ultrasonic homogenizer to accelerate cell lysis and centrifugated at 10,000 g for 10 min to pellet the cell debris. The supernatant containing isolated protein was then collected, and the protein concentration in each sample was determined using a detergent-compatible (DC) protein assay kit (Bio-Rad, Hercules, CA). Every sample had its protein concentration measured twice with the results then averaged, to ensure accurate measurement. Next sample preparation steps involved dilution to a concentration of 300 µg/ml in double-distilled water (ddH<sub>2</sub>O) with 5× Laemmli buffer containing 5% β-mercaptoethanol (BioShop Canada, Burlington, ON) followed by boiling the samples for 5 min (Laemmli, 1970). Finally, 50 µl of each sample containing 15 µg of total protein were loaded alongside BLUelf

protein ladder (FroggaBio, Buffalo, NY) into SDS-PAGE gels consisting of a 4% stacking and 8% resolving gel. The samples were first allowed to stack at the interface between the stacking and resolving gel, achieved by electrophoresis at 55 V for about 30 minutes. The voltage was then increased to 110 V for approximately 2 hours, with electrophoresis stopped after the 35 kDa band of the protein ladder had run off the gel.

Prior to detection of hERG, separated proteins within the gels were transferred to a polyvinylidene difluoride (PVDF) membrane using a wet transfer system (Bio-Rad, Hercules, CA). A 1-liter preparation of PVDF transfer buffer consisted of 80% (v/v) ddH<sub>2</sub>O, 20% (v/v) methanol, 25 mM Tris, and 192 mM glycine (BioShop Canada, Burlington, ON), was stored at 4°C and used up to 2 times before being discarded. The transfer was performed overnight at 30 V in a cold room (4°C) with an ice pack in the transfer bath to keep bath resistance to a minimum and ensure efficient protein transfer.

After the transfer, the membranes were first blocked with 5% (w/v) nonfat milk (Thermo-Fisher Scientific, Waltham, MA) in tris-buffered saline with Tween 20 (TBST) for 1 h at room temperature (RT, 22±1°C). A 1-liter preparation of TBST contained 100 ml of a concentrated 10× TBS solution (1.21% (w/v) Tris and 8.77% (w/v) 1.5 M HCl in ddH<sub>2</sub>O) diluted in 899 ml of ddH<sub>2</sub>O with the addition of 1 ml of Tween 20. Membranes were cut along the 63 kDa line on the protein ladder and incubated for 1.5 hr at RT with primary antibodies against the hERG protein (F-12) (sc-377; Santa Cruz, Dallas, TX) and β-actin (AC40) (A4700; Sigma Aldrich, St. Louis, MO). Primary antibody solutions contained 5 ml of 5% (w/v) nonfat milk in TBST with the addition of the anti-hERG primary (1:500) or anti-β-actin (1:1500). The membranes were then washed 3 times for 5 minutes each with TBST, before being incubated for 1 hr at RT with a horse anti-mouse horseradish peroxidase-conjugated secondary antibody (7076; Cell Signaling, Danvers, MA).

Finally, the membranes were incubated with an Amersham enhanced chemiluminescence kit (Cytiva, Marlborough, MA), using 1 ml of combined two-part solution per single 5.8×8.5 cm membrane. The membranes were then loaded into light-proof cassettes, and the protein bands visualized using X-ray film (Fujifilm, Tokyo, Japan) with an average exposure time of 5-10 min.  $\beta$ -actin was used to ensure equal protein loading across samples and as a normalization factor for densitometry analysis of the Western blotting results. For densitometry analysis, films containing Western blotting results from several independent experiments were scanned using an Epson V700 flatbed scanner (Epson, Nagano, Japan) and saved as tiff files. Prior to analysis, image data was inverted using Photoshop (Adobe, San Jose, CA) to allow for compatibility with ImageLab Software (Bio-Rad, Hercules, CA). Upper band intensities representing mature hERG protein were normalized to their respective actin band intensities and then normalized to the control sample on the same gel. Densitometry data are presented using line-and-symbol plots as mean $\pm$ S.D.

### **2.3 Patch Clamp Electrophysiology**

To record  $I_{hERG}$  in hERG-HEK cells, the whole-cell voltage-clamp method was employed. Axopatch 200B amplifier and DigiData 1440A digitizer were used to record membrane currents and visualize the results on a computer (Molecular Devices, San Jose, CA). Clampex 10.7 was used to create voltage protocols and acquire data (Molecular Devices, San Jose, CA). The current was sampled at 5 kHz and filtered at 1 kHz. Liquid junction potential was calculated at +5.0 mV using the JPCalcW tool within the Clampex software and was not compensated. Pipettes used for electrophysiological recordings were pulled from thin-walled borosilicate glass filaments (World Precision Instruments, Sarasota, FL) using a Sutter P1000 micropipette puller (Sutter Instrument, Novato, CA). The tip of the recording pipette was then polished using heat treatment to a target resistance of  $\sim$ 2 M $\Omega$  when filled with pipette solution. The pipette solution contained (in mM) 135

KCl, 5 EGTA, 5 MgATP, and 10 HEPES (pH adjusted to 7.2 with KOH). The bath solution contained (in mM) 135 NaCl, 5 KCl, 2 CaCl<sub>2</sub>, 1 MgCl<sub>2</sub>, 10 glucose, and 10 HEPES (pH adjusted to 7.4 with NaOH). Series resistance ( $R_s$ ) was compensated and leak subtraction was not used. Cells had a capacitance of ~15 pF, which was compensated. For transiently transfected cells, either HEK293 or H9c2, a blue laser was used to stimulate GFP fluorescence and identify cells successfully co-transfected with WT or mutant hERG cDNA. All recordings were performed at RT and in normal atmospheric conditions.

Families of hERG current traces were recorded from a holding potential of -80 mV using a voltage protocol with 4-second depolarizing steps to voltages between -70 and +70 mV in 10 mV increments followed by 5-second repolarizing step to -50 mV before returning to the holding potential. The interval between subsequent sweeps was set to 15 s. This protocol takes advantage of the unique gating kinetics of hERG, with maximum tail current amplitudes reached following initial depolarization to voltages positive to 10 mV. As such, tail current amplitudes elicited by a prior depolarizing step to +50 mV were used in the analysis of  $I_{hERG}$ . Analysis of patch-clamp recordings was performed using Clampfit (Molecular Devices, San Jose, CA), and the data was further processed in Microcal Origin 6.0 and 9.0 (OriginLab, Northampton, MA). To measure tail current amplitudes, cursors 1 and 2 were placed during the holding potential to quantify the baseline current, while cursors 3 and 4 were positioned 50 ms and 250 ms after the start of the repolarizing voltage step. Tail current amplitudes were calculated by subtracting the peak current between cursors 1 and 2 from that between cursors 3 and 4. To calculate half-maximal inhibitory concentration ( $IC_{50}$ ) values and Hill coefficients of concentration-response relationships,  $I_{hERG}$  values were averaged and fitted to the Hill equation. Patch-clamp data are presented as mean $\pm$ S.D. in a scatterplot or a box plot with overlapping data points.

For acute concentration-response experiments, cells were first recorded in the control bath solution. A drug, as indicated, was then added at increasing concentrations and current inhibition was allowed to achieve a steady state before the tail currents were recorded. This step was repeated with increasing concentrations of the drug until a concentration-dependence curve could be constructed. In this case, the currents obtained at each drug concentration were normalized to the control  $I_{\text{hERG}}$  tail current magnitude of each recorded cell. To investigate the concentration-response relationships following long-term culture with a drug, several groups of cells were cultured overnight with varying concentrations of the drug before  $I_{\text{hERG}}$  was recorded. Here,  $I_{\text{hERG}}$  tail current amplitudes were normalized to each cell's respective membrane capacitance value to obtain a current density value that was then plotted to create a concentration-dependence curve.

## 2.4 Drugs and Treatments

Proteinase K (PK) was purchased from Sigma-Aldrich, St. Louis, MO. Immediately prior to the treatment, cells were washed with  $\text{Ca}^{2+}$ -free D-PBS. They were then incubated in a buffer containing 10 mM HEPES, 150 mM NaCl, and 2 mM  $\text{CaCl}_2$  (pH 7.4) without (control) or with 200  $\mu\text{g/ml}$  PK at 37°C for 20 mins. Treatment was stopped by adding 6 mM PMSF in ice-cold PBS. Cells were centrifugated and resuspended in normal culture medium, then used for patch-clamp recordings or Western blotting.

AMIO and E-4031 were purchased from Cayman Chemical, Ann Arbor, MI. Verapamil was purchased from Sigma-Aldrich, St. Louis, MO. N-desethylamiodarone (DEA) was purchased from Toronto Research Chemicals, Toronto, ON. As indicated for each experiment, various concentrations of drugs were either added acutely through bath perfusion or as part of an overnight (chronic) treatment of approximately 16 hrs. For acute recordings, steady-state current inhibition was achieved before raising the drug concentration or attempting to wash out its blocking effects

with a drug-free bath solution. Chronic treatment was achieved by dissolving the drug's stock solution to a desired concentration in culture medium. To wash out the chronic effects, cells were washed twice with Ca<sup>2+</sup>-free D-PBS. They were then collected by trypsinization and resuspended in normal culture medium (see 2.1 Cell Culture and Molecular Biology) for patch-clamp experiments or detached using a rubber cell scraper Western Blot Analysis.

Brefeldin A (BFA) was purchased from Sigma-Aldrich, St. Louis, MO. In experiments investigating the decay of the hERG upper band, BFA was added to either the control culture or to those pretreated with AMIO overnight. For AMIO-pretreated cells, the next-day treatment consisted of either the washout of AMIO from the culture and addition of fresh media containing only 10 µM BFA or the replacement of the AMIO-containing media by fresh media containing both the AMIO and BFA. The cells were then collected for patch-clamp or Western blot experiments. Bafilomycin (Baf) was purchased from BioShop Canada, Burlington, ON.

## **2.5 Statistical Analysis**

Statistical analysis was performed using GraphPad Prism 8 (GraphPad Software, Boston, MA). To determine whether variation between the control and experimental groups were statistically significant, one-way analysis of variance (ANOVA) with Tukey's post hoc test were used. A *p* value of <0.05 was considered statistically significant.

## Chapter 3 – Results

### 3.1 Chronic AMIO inhibits $I_{hERG}$ but does not affect mature hERG channel expression

hERG channel function can be pharmacologically modulated by directly blocking channel conductance, reducing channel expression on the membrane surface, or both (Rajamani et al., 2006). Since only acute  $I_{hERG}$  block by AMIO had been described in literature (Kauthale et al., 2015; Kiehn et al., 1999b; McPate et al., 2008; Ridley et al., 2004; Zhang et al., 2016; Zhang et al., 2010), we investigated the effects of chronic application on hERG channel function and expression by utilizing the whole-cell voltage-clamp method or Western blotting, respectively. For this experiment, various concentrations of AMIO were added to culture media and hERG-HEK cells were incubated with the drug overnight (16 h). To ensure that the drug was completely washed out of the extracellular space, the cells pretreated with AMIO were washed twice with D-PBS before being trypsinized, centrifuged at 1000 g for 5 min, and resuspended in standard culture medium.  $I_{hERG}$  recordings were performed in drug-free external solution. The upper panel of Figure 6 demonstrates the concentration-dependent inhibition of  $I_{hERG}$  in response to culture with increasing AMIO concentrations. The  $EC_{50}$  value for AMIO-induced block was 0.32  $\mu$ M with a Hill coefficient of 0.7. Since no drug was present during electrophysiological recordings, these results pointed to a potential effect of overnight-applied AMIO on mature channel expression or trafficking to the membrane.

With the above results in mind, we investigated whether chronic AMIO application may have a similar inhibitory effect on mature hERG channel expression comparable to drugs such as fluoxetine, probucol, digoxin, pentamidine, or arsenic trioxide. Long-term treatment with these agents has been shown to predominantly decrease  $I_{hERG}$  by reducing the number of channels at the

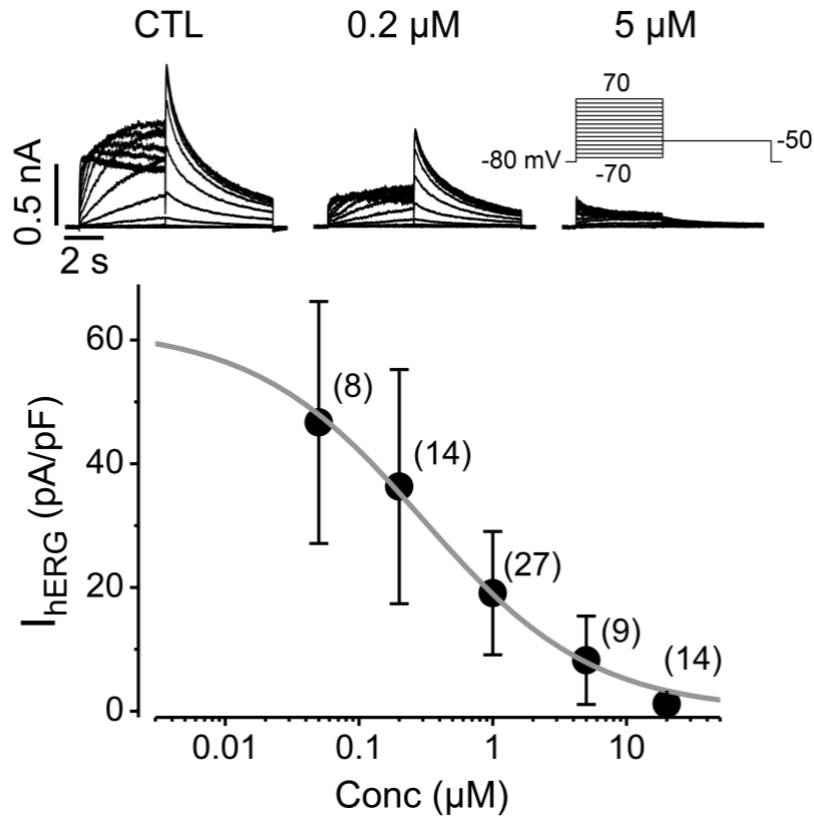


**Figure 6. Overnight AMIO application decreases  $I_{hERG}$  recorded in hERG-HEK cells in drug-free conditions.**

Upper panel: Families of  $I_{hERG}$  traces recorded using the voltage protocol above. Currents were recorded from cells after overnight (16 h) culture without (control, CTL) or with 0.2  $\mu\text{M}$  and 5  $\mu\text{M}$  AMIO. Lower panel: Concentration-response relationships for overnight culture with AMIO-mediated  $I_{hERG}$  inhibition.  $I_{hERG}$  is plotted against AMIO concentrations, and data were fitted to the Hill equation ( $n=8-27$ ). There is a clear concentration-dependent inhibition of  $I_{hERG}$  overnight-applied AMIO despite the recordings being performed in drug-free conditions.

membrane that are available to conduct  $I_{hERG}$  (Dennis et al., 2012; Ficker et al., 2004; Guo et al., 2007; Rajamani et al., 2006; Wang et al., 2007). To probe this mechanism of current modulation, we used Western blot analysis. WT hERG detection on a Western blot yields two distinct bands, lower band at 135 kDa and upper band at 155 kDa. The former represents the immature core-glycosylated channels that are contained in the endoplasmic reticulum and are therefore non-conductive. On the other hand, the upper band represents the mature fraction of the channel proteins – fully glycosylated and trafficked to the membrane – that pass  $I_{hERG}$ . While we expected to see a gradual reduction in the density of the upper band with increasing AMIO concentrations, to our surprise, there was no effect on mature channel expression at any of the concentrations used. A representative Western blot of hERG expression in whole cell lysates of hERG-HEK cells treated with 0.2  $\mu$ M, 1  $\mu$ M, or 5  $\mu$ M AMIO overnight (16 h) in Figure 7A shows that the intensity of the upper band remained unchanged across all samples.

Finally, to ensure that the detected mature channels were in fact localized to the membrane, cells pretreated with 1  $\mu$ M AMIO overnight were then subjected to a PK treatment in the morning. Only the surface-expressed proteins are subject to PK cleavage due to the membrane-impermeable nature of this protease. Having abolished only the upper band and not the lower band in both the control and AMIO-pretreated cells (Fig. 7B), we were able to confirm the localization of AMIO-blocked channels to the plasma membrane. While their conductivity was lost, likely due to a direct interaction with the mature channel protein, the channels remained membrane-bound. Therefore, these data suggest a unique interaction between the hERG channel and AMIO, as persistent inhibition of the current after overnight culture with the drug and removal of the drug from culture media did not rely on changes in mature channel expression levels.

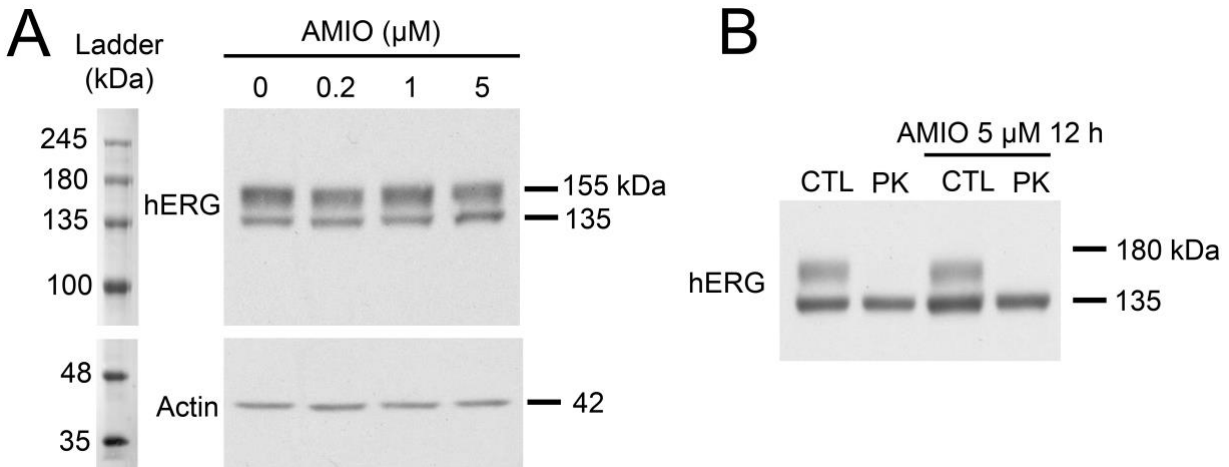


**Figure 7. Mature hERG expression in hERG-HEK cells remained unaffected following overnight culture with AMIO.**

A. Representative Western blot images displaying the effects of overnight AMIO exposure on mature hERG channel expression (n=5). Increasing AMIO concentrations did not affect the expression of the upper hERG band; B. Mature hERG channel proteins from both control cells and AMIO-treated cells are susceptible to extracellularly applied PK treatment. hERG-HEK cells were cultured without (control, CTL) or with 1 μM AMIO overnight. Both control and AMIO-pretreated cells were subjected to 200 μg/ml PK treatment for 20 min. Cells were resuspended in regular drug-free medium and used for Western blot analysis (n=3). These results indicate that the upper hERG band in AMIO-pretreated cells represented the membrane-bound fraction of the channels.

### 3.2 AMIO irreversibly inhibits $I_{hERG}$

To further probe the persistence of AMIO-mediated  $I_{hERG}$  inhibition, we began by taking a closer look at its acute effects. Figure 8A demonstrates the concentration-dependent inhibition of  $I_{hERG}$  by acutely-applied AMIO. The left panel contains representative  $I_{hERG}$  traces recorded from the same cell in the control condition as well as after the addition of 0.2  $\mu\text{M}$  followed by 5  $\mu\text{M}$  AMIO. Above the traces, the voltage protocol used for whole-cell patch-clamp recordings is shown. For this experiment, a control current recording was first obtained for each of the cells. Increasing concentrations of AMIO (0.05  $\mu\text{M}$ , 0.1  $\mu\text{M}$ , 0.2  $\mu\text{M}$ , 0.5  $\mu\text{M}$ , 1  $\mu\text{M}$ , 5  $\mu\text{M}$ , 10  $\mu\text{M}$ , and 20  $\mu\text{M}$ ,  $n=5-9$  at each concentration) were then applied by bath perfusion and peak  $I_{hERG}$  tail current was recorded once inhibition achieved a steady state. Relative  $I_{hERG}$  magnitudes were plotted against their corresponding AMIO concentrations as well as fit to the Hill equation yielding an  $IC_{50}$  value of 0.22  $\mu\text{M}$  and a Hill coefficient of 0.96. The summarized concentration-response relationship for acutely applied AMIO is presented in the right panel of Fig. 8A. In agreement with previous reports by other laboratories, acutely-applied AMIO blocked  $I_{hERG}$  in a concentration-dependent manner, with the  $IC_{50}$  and Hill coefficient also consistent with literature (Kauthale et al., 2015; McPate et al., 2008; Ridley et al., 2004; Zhang et al., 2016). Of note, the  $EC_{50}$  of the chronic block was close to the acute  $IC_{50}$  value – 0.32  $\mu\text{M}$  and 0.22  $\mu\text{M}$ , respectively – although the lower Hill coefficient of chronically-applied AMIO indicated reduced binding cooperativity.

So far, our results have identified that AMIO-mediated block of  $I_{hERG}$  is maintained even after its removal from the extracellular environment, despite the lack of an effect on mature surface channel expression of hERG. Therefore, we investigated whether the drug may permanently associate with and inhibit the function of the hERG channel, by probing the washout properties of AMIO. In figure 8B,  $I_{hERG}$  values immediately prior to and following the addition of

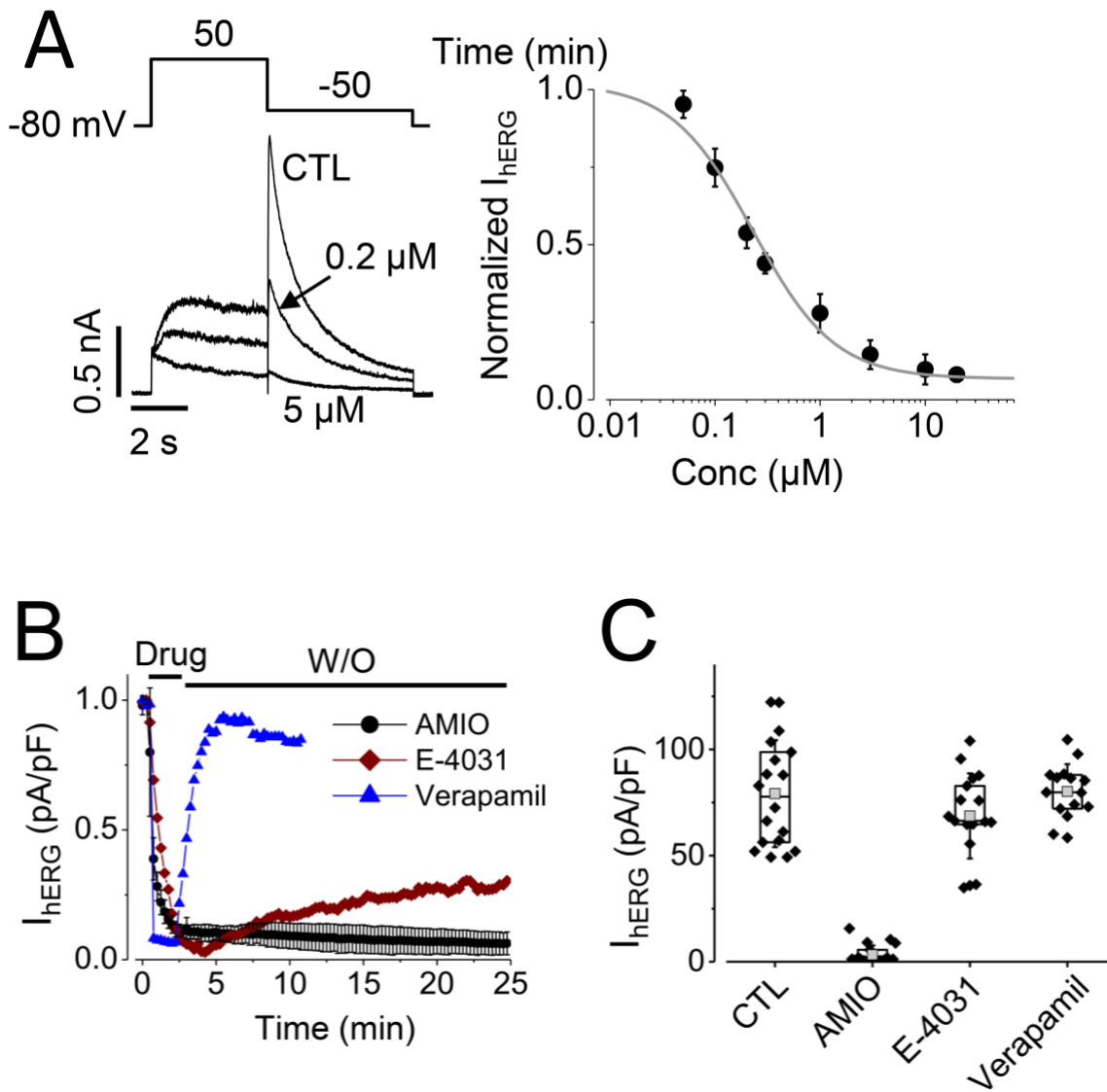


**Figure 8. AMIO irreversibly inhibits  $I_{hERG}$ .**

A. Acute bath perfusion with AMIO inhibits  $I_{hERG}$  in a concentration-dependent manner. Left panel: Representative current traces recorded from the same cell in the control condition, and with 0.2  $\mu$ M and 5  $\mu$ M AMIO. Right panel: Concentration-response relations of AMIO-induced  $I_{hERG}$  inhibition;  $I_{hERG}$  is plotted against AMIO concentrations; data were fitted to the Hill equation. B. Normalized  $I_{hERG}$  plotted against time during AMIO application and washout. Following steady-state block,  $I_{hERG}$  did not recover from 5  $\mu$ M AMIO-mediated inhibition. Recovery from 1  $\mu$ M E-4031- or 5  $\mu$ M verapamil-mediated inhibition was partial or nearly complete. C.  $I_{hERG}$  recorded in drug-free condition from cells cultured overnight (16 h) in the control condition and with 5  $\mu$ M AMIO, 1  $\mu$ M E-4031, or 5  $\mu$ M verapamil.  $I_{hERG}$  were normalized using each cell's recorded membrane capacitance value.

5  $\mu\text{M}$  AMIO are plotted against time. As can be seen in Fig. 8B, the current was first allowed to achieve a complete block before the bath solution was switched to a drug-free one. Despite 25 minutes of continuous membrane stimulation using the protocol from Fig. 8A and perfusion with a drug-free bath solution, no current recovery was observed (Fig. 8B,  $n=5$ ). These data further corroborated the evidence of a permanent drug-channel interaction between AMIO and hERG. However, to demonstrate the uniqueness of this interaction, we employed other well-characterized hERG-blocking agents. To begin with, we applied E-4031, a potent  $I_{\text{hERG}}$  blocker of the methanesulfonanilide family (Helliwell et al., 2023). After achieving a steady-state block, current recovery from the effects of 1  $\mu\text{M}$  E-4031 was slow but steady over the 25 minutes of perfusion with a drug-free bath solution (Fig. 8B). Next, we tested verapamil, an antiarrhythmic initially approved as a  $\text{Ca}^{2+}$  channel blocker, but later also shown to potently inhibit  $I_{\text{hERG}}$  (Zhang et al., 1999).  $I_{\text{hERG}}$  recovered to  $\sim 90\%$  of the control value following a block elicited by an acute application of 5  $\mu\text{M}$  verapamil. This occurred on a much faster time-course than either E-4031 or AMIO, with current recovery taking about 5 min following the switch to a drug-free bath solution (Fig. 3B). Unlike AMIO, however, both compounds showed current recovery, be it slow or fast, emphasizing the uniqueness of the irreversible AMIO-induced hERG inhibition.

Next, we aimed to establish whether the persistent effect of acutely-applied AMIO on  $I_{\text{hERG}}$  was implicated in the loss of conductance observed after overnight treatment. To this end, we cultured hERG-HEK cells overnight in the absence (CTL) or presence of 5  $\mu\text{M}$  AMIO, 1  $\mu\text{M}$  E-4031, or 5  $\mu\text{M}$  verapamil. As described above, cells were washed twice with  $\text{Ca}^{2+}$ -free D-PBS and trypsinized, before being loaded into the perfusion chamber. All recordings were performed under conditions of continuous perfusion with a drug-free bath solution. As expected, E-4031- and verapamil-pretreated cells recovered to the control  $I_{\text{hERG}}$  amplitudes. On the other hand, AMIO

pretreatment resulted in a complete and irrecoverable loss of  $I_{hERG}$  conductance. Current densities recorded from controls or following washout of an overnight application of AMIO, E-4031, or verapamil-pretreated groups are summarized in Figure 8C. These data demonstrate the similar hERG-blocking effects of acutely- and chronically-applied AMIO and further support the evidence for its irreversible interaction with mature hERG channels located on the membrane surface.

We also probed the state-dependence of AMIO-induced channel block. To do so, a shorter voltage protocol was created, with the depolarizing step to +50 mV and the repolarizing step to +50 mV reduced to 200 ms. The duration of the pulse interval – time spent at the holding potential – was then modified to last 0.6, 2, or 20 s. This voltage protocol was then applied during acute bath perfusion with an external solution containing 3  $\mu$ M AMIO and channel opening was stimulated at different pulse intervals to investigate the use- and frequency-dependence of AMIO-mediated block. Representative traces recorded at a 2-second pulse interval in the control condition and 20, 40, and 60 s after the application of AMIO are presented in Figure 9A. In Figure 9B, relative  $I_{hERG}$  is plotted against time, detailing the relationship between the frequency of channel opening and the rate at which the AMIO-mediated block develops. As can be appreciated, AMIO displayed a strong use- and frequency-dependence, as channel opening was required for the development of the block and shorter pulse intervals led to a more rapid blockade of the channel. This is consistent with previous literature reports of AMIO preferentially binding to the hERG channel in the open and/or inactivated state (Zhang et al., 2016).

### **3.3 The effects of AMIO on mutant hERG channels**

Aromatic amino acid residues Y652 and F656 of the S6 domain project into the pore cavity, are responsible for the abundant high-affinity drug-hERG interactions, and preferentially bind compounds that can access the inner vestibule of the pore when the channel is in the open

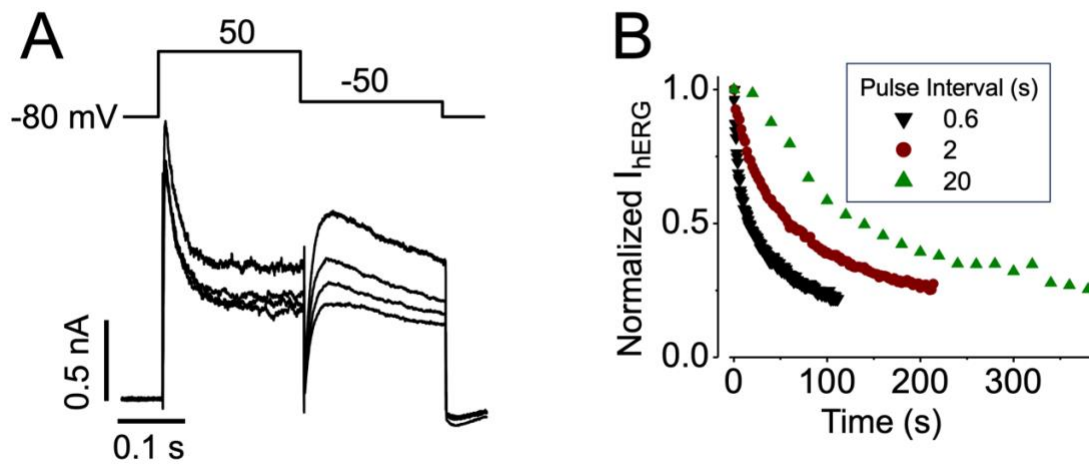


**Figure 9. AMIO-induced block of  $I_{hERG}$  is frequency- and use-dependent.**

A. Development of  $I_{hERG}$  inhibition under acute bath perfusion with 3  $\mu\text{M}$  AMIO and with repetitive pulsing using the protocol presented above with a pulse interval of 2 s. Current traces at 0, 20, 40 and 60 s time points recorded from the same cell are shown. The degree of block continually increased as a function of time. B. Frequency- and use-dependent inhibition of  $I_{hERG}$  by 3  $\mu\text{M}$  AMIO.  $I_{hERG}$  inhibition by 3  $\mu\text{M}$  AMIO during repetitive pulsing with pulse intervals of 0.6 s, 2 s, and 20 s is shown.  $I_{hERG}$  at each recorded time point was normalized to the initial amplitude recorded from the same cell, normalized  $I_{hERG}$  is plotted against time. AMIO requires channel opening to block hERG conductance, with more frequent opening resulting in faster development of block.

conformation. Mutations to these residues have been shown to dramatically reduce hERG blockers' affinity for channel binding (Kamiya et al., 2001; Lees-Miller et al., 2000; Lefevre et al., 1997; Mitcheson et al., 2000a; Sanchez-Chapula et al., 2003; Sanchez-Chapula et al., 2002). Furthermore, mutations in the S5-S6 pore linker that result in inactivation-deficient hERG channels, such as S620T and S631A, have also been reported to attenuate the channel's drug binding affinity (Chen et al., 2002; Kamiya et al., 2001; Mitcheson et al., 2000a; Sanchez-Chapula et al., 2002). Finally, involved in shaping hERG's deactivation kinetics, both the N- and C-terminal regions of the channel have also been implicated in drug interactions. However, the binding sites for AMIO on the hERG channel have not been studied extensively, and the site responsible for the irrecoverable block observed in this study remains unknown. Therefore, we induced heterologous expression of mutant hERG channels in HEK293 cells to probe the amino acid residues crucial for the AMIO-hERG interaction as well as to investigate whether any of the mutations might attenuate the strength of the drug-channel interaction. To this end, mutants containing an N-terminal deletion ( $\Delta$ 2-354) or a C-terminal truncation ( $\Delta$ C-1073) were created to eliminate the majority of potential binding sites in these intracellular regions. To investigate the involvement of residues previously reported to confer hERG's high affinity for drug interactions, point mutations in the common drug-binding sites (Y652A, F656V) and the pore linker (S620T, S631A) were introduced. Successfully transfected cells were identified by using GFP fluorescence. AMIO was acutely applied through bath perfusion, with cells in each group first recorded for their control current followed by recordings with increasing AMIO concentrations in the bath solution. The data were then fitted to the Hill equation. Figure 10A illustrates the concentration-response relationships of AMIO with the WT as well as mutant hERG channels described above. Figure 10B summarizes the  $IC_{50}$  values of AMIO-induced block obtained either from WT or mutant hERG channels. The N- and C-

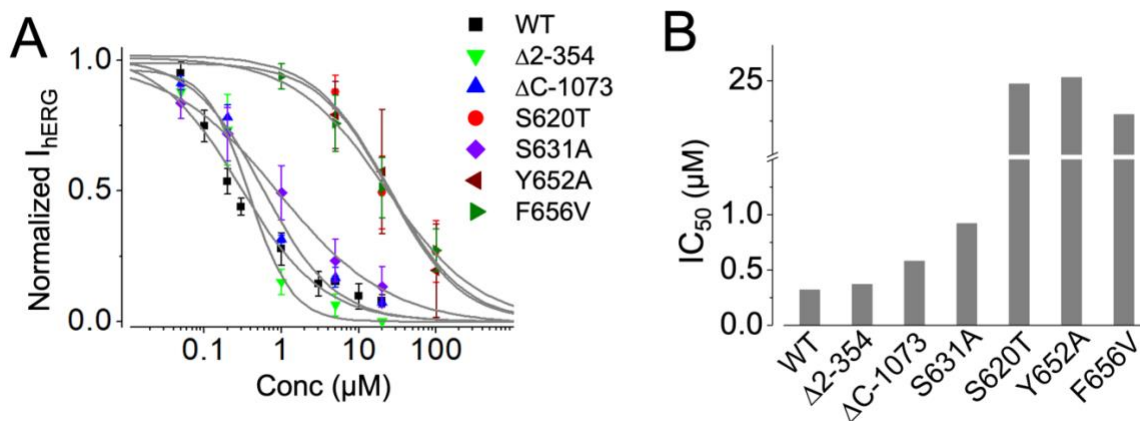


**Figure 10. AMIO shares binding sites with other class III agents.**

A. Concentration-response relationships of acute bath-applied AMIO for WT and mutant hERG channels. Normalized  $I_{hERG}$  values were plotted against AMIO concentrations, and the data were fitted to the Hill equation. Only the S620T, Y652A, and F656V mutants showed a marked increase in the  $IC_{50}$  values of block B. Summarized  $IC_{50}$  values of AMIO-induced  $I_{hERG}$  inhibition of WT and mutant hERG channels.

terminal mutations failed to attenuate AMIO binding to any appreciable degree ( $\Delta 2-354$ ,  $IC_{50}=0.37$   $\mu M$ ,  $n=4$ ;  $\Delta C-1073$ ,  $IC_{50}=0.58$   $\mu M$ ,  $n=4$ ). Inactivation deficient mutants displayed a variable response, with the S631A mutant showing a moderate attenuation in binding affinity ( $IC_{50}=0.93$   $\mu M$ ,  $n=4$ ), while the S620T mutation dramatically reduced channel binding by AMIO ( $IC_{50}=24.8$   $\mu M$ ,  $n=3$ ). Finally, as we anticipated, mutations in both of the common drug binding sites resulted in a similarly drastic reduction in AMIO's hERG-blocking activity (Y652A,  $IC_{50}=25.2$   $\mu M$ ,  $n=5$ ; F656V,  $IC_{50}=22.9$   $\mu M$ ,  $n=5$ ). While AMIO occupies the same binding sites as other open-channel hERG-blockers – as demonstrated by site-directed mutagenesis – none of the mutations probed in this study were successfully able to attenuate the irreversibility of the drug-channel association. These data indicate that the irrecoverable blockade of  $I_{hERG}$  by AMIO occurs through a separate and unique mechanism that has not been previously described.

### **3.4 $I_{hERG}$ recovery in AMIO-treated cells is dependent on newly made channels**

Seeing as  $I_{hERG}$  did not recover following AMIO-induced block, we investigated current recovery dynamics on a broader time-scale as a function of naturally-occurring channel turnover. To test whether recovery of AMIO-inhibited  $I_{hERG}$  was dependent on synthesis and forward trafficking of new channels, we treated hERG-HEK cells with 5  $\mu M$  AMIO overnight. At the 0 h timepoint, AMIO-pretreated cells had their media replaced with the control medium, and the current was allowed to recover. Samples were then collected for whole-cell voltage-clamp recordings at 0, 1, 3, 6, and 20 h points. Figure 11A illustrates the recovery dynamics of  $I_{hERG}$  following the removal of an overnight AMIO application from the extracellular environment. As can be seen,  $I_{hERG}$  recorded from AMIO-pretreated cells consistently increased throughout the 20 h of observation. As we had not been able to wash out the AMIO-induced blockade of  $I_{hERG}$ , we hypothesized that current recovery may in fact be reliant on channel turnover to remove the

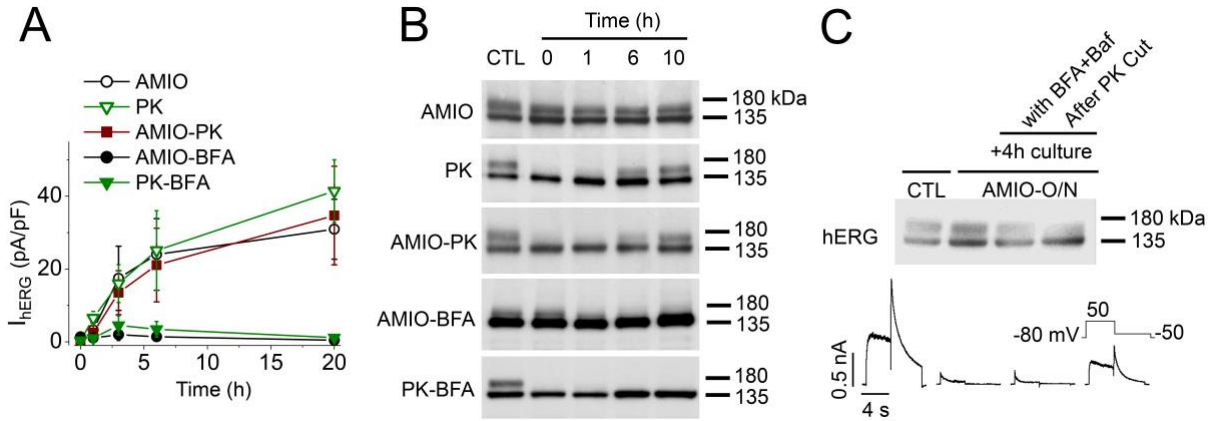


**Figure 11. Recovery of  $I_{hERG}$  from AMIO treated cells relies on newly trafficked mature channels.**

A.  $I_{hERG}$  recovery in AMIO-pretreated cells, control cells treated with PK, and AMIO-pretreated cells treated with PK and cultured in drug-free medium, as well as AMIO-pretreated cells and PK treated control cells cultured in the presence of forward trafficking inhibitor BFA (10  $\mu$ M). AMIO-pretreated cells, PK treated control cells, and AMIO-pretreated cells treated with PK showed similar current recovery time courses ( $p < 0.05$  at 3, 6, and 20 h time points). BFA abolished  $I_{hERG}$  recovery in both the AMIO-pretreated and PK treated control cells. B. Western blot images of mature hERG protein expression (upper band, 155 kDa) in the same treatment conditions as A. The upper hERG band did not change in AMIO-pretreated cells. AMIO-pretreated and control cells treated with PK initially abolished the upper band but recovered it overtime. The upper band slowly decayed in AMIO-pretreated cells cultured with BFA and did not recover at all in control cells treated with PK followed by culture with BFA. Recovery of  $I_{hERG}$  appears dependent on forward channel trafficking to the membrane. C. Upper panel: Western blot images of mature hERG expression in control cells, cells pretreated with 5  $\mu$ M AMIO, AMIO-pretreated cells further cultured with BFA and Bafilomycin (BFA+Baf) for 4 h, and AMIO-pretreated cells treated with PK and further cultured for 4 h. Lower panel: Representative  $I_{hERG}$  traces recorded from groups of cells corresponding to the upper panel ( $n=5-9$  cells from 3 independent experiments). The upper band in AMIO-pretreated cells represented non-conductive mature hERG channels, however, the recovered upper band in AMIO-pretreated PK-treated cells was associated with a renewed  $I_{hERG}$  conductance.

inhibited/damaged channels from the membrane surface and replace them with functionally intact ones. Therefore, we compared the time-course of  $I_{hERG}$  recovery of AMIO-pretreated cells with that of the cells subjected to a PK treatment as current recovery following extracellular PK application is entirely dependent on channel synthesis and forward trafficking. Intriguingly, current recovery dynamics of both the AMIO-pretreated and PK-treated cells turned out extremely close ( $p > 0.05$  at 3, 6, 20 hrs), indicating the reliance on newly made channels for recovery of AMIO-inhibited  $I_{hERG}$  (Fig. 11A). These findings were further corroborated by PK treatment of AMIO-pretreated cells, whereby the recovery time-course remained unchanged (Fig. 11A). Brefeldin A (BFA) is a fungal metabolite that disrupts anterograde protein transport between the ER and Golgi, thus preventing the maturation and trafficking of hERG channels to the membrane (Wood et al., 1991). Therefore, we confirmed the reliance on forward channel trafficking by introducing 10  $\mu$ M BFA to the AMIO-pretreated or PK-treated groups and completely abolishing current recovery in both groups (Fig. 11A). Taken together, these data correlate PK-mediated cleavage of hERG channels to an irrecoverable inhibitory effect of AMIO, pointing to a drug-channel interaction that may induce a structural change within the protein beyond simple blockade.

Next, we investigated the dynamics of  $I_{hERG}$  recovery as dependent on mature hERG channel expression levels. To this end, the same experimental groups as used in Fig. 11A were collected for Western blot analysis in the control condition as well as at 1, 6, and 10 h time points. Figure 11B displays representative Western blot images obtained from these experiments. As seen in Fig. 11B, the expression level of mature hERG channels remained unchanged throughout the experiment, while the current recovered steadily over 20 h of sample collection (Fig. 11A). On the other hand, the upper band was first abolished in the PK-treated and AMIO-pretreated PK-treated groups, with similar  $I_{hERG}$  recovery dynamics as the AMIO-pretreated group (Fig. 11A, B). Taken

together, these data indicate that the upper band in the AMIO-pretreated group represents, in varying fractions, both the AMIO-inhibited and newly made channels. The fraction of the newly made channels increases progressively after the washout of AMIO due to forward trafficking, while the AMIO-inhibited channels are being internalized. Removal of forward trafficking by 10  $\mu$ M BFA in the AMIO-pretreated group resulted in a gradual decay of the upper hERG band and prevented its recovery in the PK-treated group, as expected based on  $I_{\text{hERG}}$  recovery dynamics (Fig. 11A, B). Together, these experiments demonstrate that recovery of hERG conductance from AMIO-mediated inhibition relies entirely on the anterograde transport of newly made channels as the blocked ones on the membrane surface are permanently incapacitated.

Finally, we aimed to reinforce our evidence for permanent functional incapacitation of hERG channels by an interaction with AMIO. As such, we treated hERG-HEK cells with AMIO overnight. The AMIO-pretreated groups then had the drug removed from culture and further cultured for 4 h with 10  $\mu$ M BFA and 1  $\mu$ M bafilomycin (Baf), a lysosomal inhibitor that slows membrane-bound channel degradation, or treated with PK and allowed to recover for 4 h. The upper panel of Figure 11C shows a representative Western blot image of hERG upper band expression in drug-free and AMIO-treated controls as well as in AMIO-pretreated BFA+Baf- and PK-treated cells. In the lower panel are representative current traces obtained from the same experimental groups.  $I_{\text{hERG}}$  was completely abolished in the AMIO-pretreated BFA+Baf-treated cells, despite the presence of an upper band and a 4-hour period in the absence of drug. Alternatively, with mature channels cleared from the surface by PK cleavage, 4-hour culture without AMIO allowed for enough newly made channels to be trafficked to the membrane to restore a robust conductance (Fig. 11C).

### **3.5 AMIO modulates the rate of mature hERG channel degradation**

As presently established, interaction with AMIO permanently inhibits mature hERG channel function. To further probe the effects of this interaction, we investigated the rate of mature channel degradation. Cells were either cultured in the control condition or pretreated with overnight AMIO. Control cells were then treated with 10  $\mu$ M BFA, with samples collected for Western blot analysis at 1, 3, 6, 9, and 12 h time points. Likewise, AMIO-pretreated cells were also treated with 10  $\mu$ M BFA either in the presence or absence of AMIO with samples collected at the same time points as above. Figure 12A shows representative Western blot images for the 3 experimental conditions, with Fig. 12B summarizing these results using densitometry analysis of hERG upper band expression. As expected, treatment with BFA revealed the natural hERG channel turnover unmasked by inhibited forward trafficking of newly made channels (Fig. 12B) (Ficker et al., 2003). On the other hand, AMIO-pretreated cells further cultured with BFA displayed a markedly accelerated rate of mature channel degradation (Fig. 12B;  $p < 0.05$  at each time point excl. CTL) with the maintenance of AMIO in the culture medium during further culture with BFA reversing this effect and returning the mature channel degradation rate to the control level (Fig. 12B;  $p > 0.05$  at each time point). These results suggest a structural change induced by an interaction with AMIO that accelerates mature channel internalization and degradation. Intriguingly, this effect was attenuated by maintaining the extracellular concentration of AMIO.

### **3.6 DEA displays a similar interaction with hERG as AMIO**

The major metabolite of AMIO, termed DEA, is known to exhibit similar therapeutic effects to its parent compound (Zhang et al., 2010). However, since both compounds are very close in structure, we hypothesized that DEA may also irreversibly inhibit  $I_{hERG}$ . Therefore, we tested

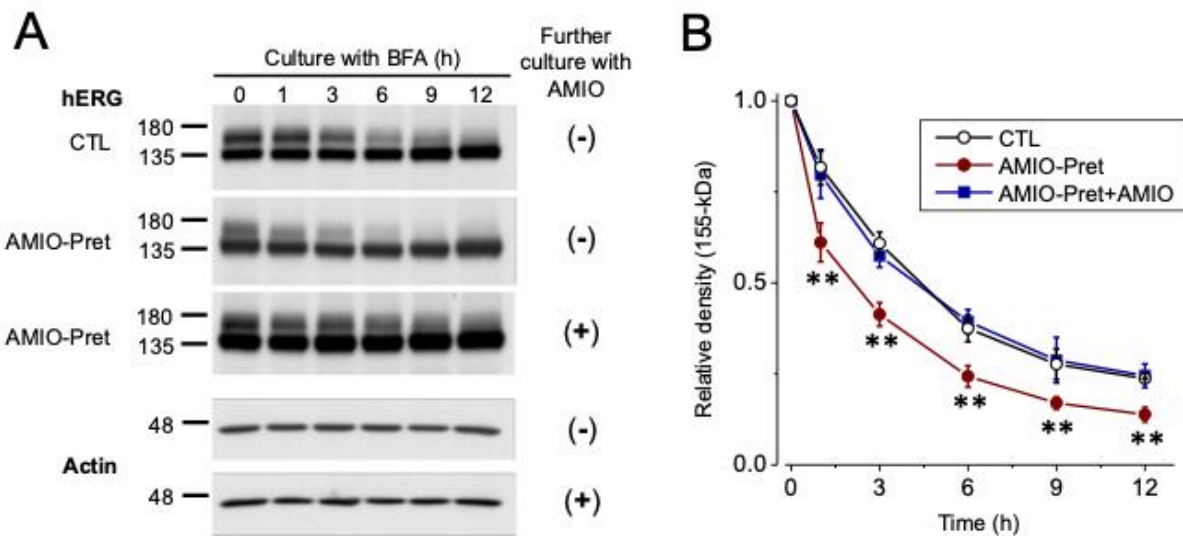


**Figure 12. Effects of AMIO on the degradation of mature hERG proteins.**

A. Western blot images demonstrating the decay of hERG upper band expression in control cells cultured with 10  $\mu$ M BFA (upper panel) or AMIO-pretreated cells further cultured in medium with BFA with (lower panel) or without 5  $\mu$ M AMIO (middle panel) for 12 hrs. B. Relative densities of the hERG upper bands using the same groups as A. Densities of the hERG upper bands at each time point were normalized to each respective sample's actin band intensity, expressed as a fraction the group's initial (0 h) value, and plotted against time (n=4). AMIO-pretreated cells further cultured with BFA but without AMIO display significantly accelerated hERG upper band decay, indicating potential structural changes due to the drug-hERG interaction.

the properties of acute and chronic blockade as well as recovery from the former. Figure 13A demonstrates representative traces of  $I_{hERG}$  recorded in the control condition and following overnight treatment with 5  $\mu\text{M}$  DEA and summarizes the concentration-response relationship of its chronic effects. Similar to AMIO-pretreated samples, cells were first washed twice with  $\text{Ca}^{2+}$ -free D-PBS, followed by trypsin treatment to collect the cells for patch-clamp recordings. All recordings of the drug's chronic effects were also performed using a drug-free bath solution. As can be seen in Fig. 13A, overnight treatment with DEA produced a concentration-dependent inhibition of  $I_{hERG}$  with an  $\text{EC}_{50}$  of 0.85  $\mu\text{M}$  and a Hill coefficient of 0.65. Concentration-dependence of DEA's acute blocking effects on  $I_{hERG}$  is presented in Figure 13B alongside representative traces recorded in the same cell in the control condition as well as following steady-state inhibition with 1  $\mu\text{M}$  and 10  $\mu\text{M}$  DEA. Again, the same methodology and voltage protocols were used as for recordings of acute AMIO-induced hERG blockade. Recordings with increasing drug concentrations are made in the same cell, with tail current amplitudes at each concentration normalized to the control recording made in each respective cell. As expected, acute bath application of DEA resulted in a concentration-dependent reduction in  $I_{hERG}$ , with an  $\text{IC}_{50}$  of 0.95  $\mu\text{M}$  and a Hill coefficient of 1.99. Next, results of an experiment probing the washout properties of 5  $\mu\text{M}$  bath-applied DEA are presented in Figure 13C. To achieve this,  $I_{hERG}$  was first allowed to achieve a steady-state inhibition by an acute application of 5  $\mu\text{M}$  DEA. Perfusion was then switched to a drug-free bath solution, and the current was allowed to recover with continuous (20 min) voltage-clamp recording. As previously observed with AMIO, DEA-blocked hERG conductance did not recover throughout the experiment. Finally, Figure 13D demonstrates a representative Western blot of the effects of overnight treatment with varying concentrations of DEA on mature hERG channel expression levels. Like AMIO, DEA did not affect the upper band

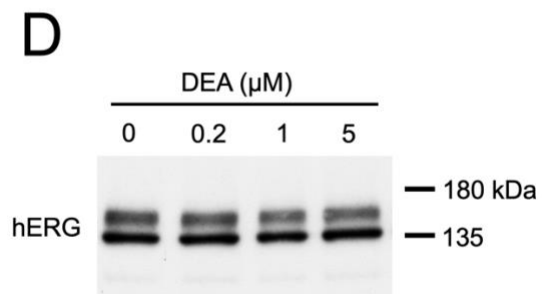
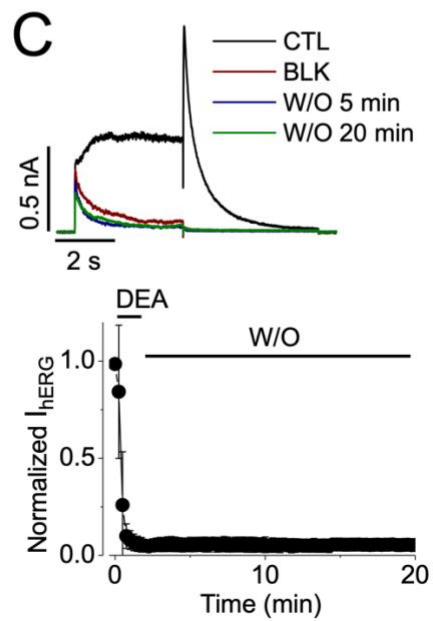
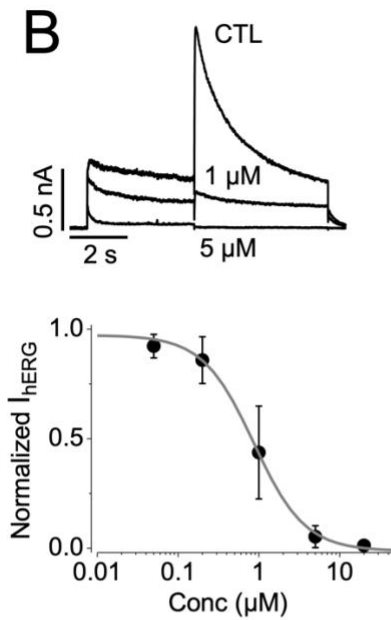
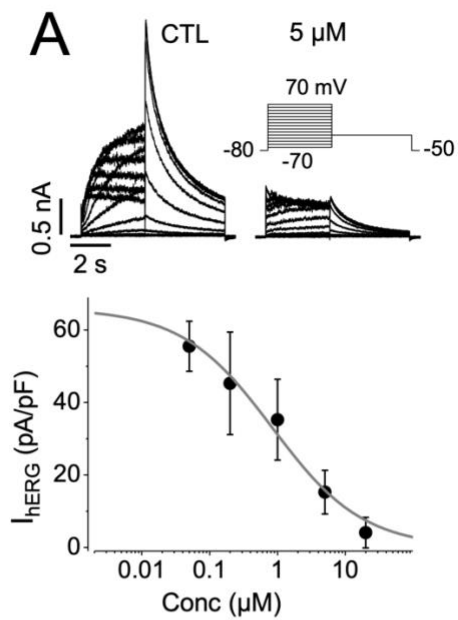


**Figure 13. DEA, the major metabolite of AMIO, also irrecoverably inhibits  $I_{hERG}$ .**

A. Effects of overnight culture with DEA on  $I_{hERG}$  recorded in drug-free conditions. Upper panel: Families of  $I_{hERG}$  traces recorded in drug-free conditions in control cells as well as cells cultured with 5  $\mu$ M DEA overnight. Lower panel: Concentration-response relationships of overnight-applied DEA and  $I_{hERG}$ .  $I_{hERG}$  was plotted against DEA concentrations and the data were fitted to the Hill equation. B. Acute  $I_{hERG}$ -inhibitory effects of DEA. Upper panel: Superimposed  $I_{hERG}$  traces recorded from the same cell in the control condition and after bath perfusion with 1  $\mu$ M and 5  $\mu$ M DEA. Lower panel: Concentration-response relationship of acute DEA-induced  $I_{hERG}$  inhibition.  $I_{hERG}$  values at each concentration were normalized to the control value recorded from each respective cell and plotted against DEA concentrations. The data were fitted to the Hill equation. C.  $I_{hERG}$  does not recover following DEA application. Upper panel: Representative  $I_{hERG}$  traces recorded in the same cell in the control condition, after achieving steady-state inhibition by 10  $\mu$ M DEA, and after 5- and 20-min periods of perfusion with a drug-free external solution. Lower panel:  $I_{hERG}$  recorded during 20 min of perfusion with a drug-free external solution following steady-state inhibition by 10  $\mu$ M DEA.  $I_{hERG}$  values normalized to each respective cell's control values are plotted against time reflecting development of DEA-mediated current inhibition and its washout. D. Western blot image of mature hERG channel expression in the control condition or following overnight culture with varying concentrations of DEA (0.2, 1, or 5  $\mu$ M).

density of the hERG protein. These results demonstrate that the principal active metabolite of AMIO has similar hERG-blocking effects to its parent compound, albeit with reduced potency.

### **3.7 hERG channels heterologously expressed in cardiomyocyte-derived H9c2 cells are similarly blocked by AMIO and DEA**

Despite HEK cells being the most frequently used expression system for electrophysiological research, including drug-hERG interactions, whether the results reliably translate to native tissue is an ongoing debate. To address this issue, we aimed to bridge the gap between the HEK- and cardiomyocyte-based models by inducing transient WT hERG expression in a rat cardiomyocyte-derived H9c2 cell line. To analyze the  $I_{\text{hERG}}$ -modulatory effects of AMIO and DEA in this expression system, we used the same methodology as described above for hERG-HEK cells. As expected, we observed concentration-dependent block of hERG channel conductance upon acute bath perfusion with AMIO with an  $IC_{50}$  of 0.39  $\mu\text{M}$  and a Hill coefficient of 0.69 (Fig. 14A, B). Once again, the association between AMIO and mature hERG channels proved persistent, with no  $I_{\text{hERG}}$  recovery observed in H9c2 cells after blockade with 10  $\mu\text{M}$  AMIO (Fig. 14C). Likewise, DEA also acutely blocked H9c2-expressed hERG channels, showing clear concentration-dependence with an  $IC_{50}$  of 0.97  $\mu\text{M}$  and a Hill coefficient of 0.74 (Fig. 14D, E).  $I_{\text{hERG}}$  also failed to recover following complete block with 10  $\mu\text{M}$  DEA (Fig. 14F). Taken together, these data point out the applicability of these results across cell lines, likely making it valid in native cardiomyocytes as well. The irrecoverable acute block of  $I_{\text{hERG}}$  by both AMIO and DEA and its chronic effects on channel expression and function are therefore expected to also apply to human ventricular tissue.

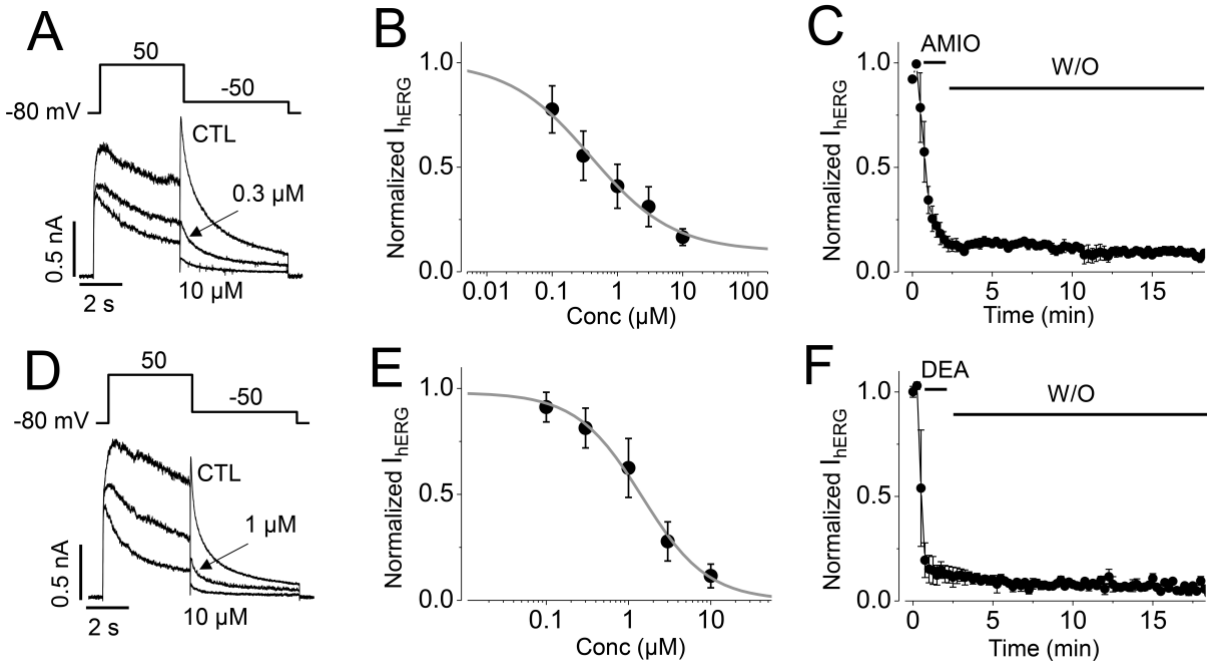


**Figure 14. Acute effects of AMIO and DEA on the currents of hERG channels heterologously expressed in H9c2 cells.**

A.  $I_{hERG}$  traces recorded from the same cell in the control condition and after acute bath application of 0.3  $\mu\text{M}$  and 10  $\mu\text{M}$  AMIO. Voltage protocol is presented above the traces. B. Concentration-response relationships of acute bath-applied AMIO and  $I_{hERG}$ .  $I_{hERG}$  values normalized to each respective cell's control value are plotted against AMIO concentrations. Data were fitted to the Hill equation. C.  $I_{hERG}$  during application of 10  $\mu\text{M}$  AMIO and ~20 min perfusion with drug-free external solution. Relative  $I_{hERG}$  values are plotted against time. D.  $I_{hERG}$  traces recorded from the same cell in the control condition and after acute bath application of 1  $\mu\text{M}$  and 10  $\mu\text{M}$  DEA. Voltage protocol is presented above the traces. E. Concentration-response relationships of acute bath-applied DEA and  $I_{hERG}$ .  $I_{hERG}$  values normalized to each respective cell's control value are plotted against DEA concentrations. Data were fitted to the Hill equation. F.  $I_{hERG}$  during application of 10  $\mu\text{M}$  DEA and ~20 min perfusion with drug-free external solution. Relative  $I_{hERG}$  values are plotted against time.

## Chapter 4 – Discussion

The propensity of the hERG channel for various drug interactions presents a considerable risk of LQTS and associated life-threatening arrhythmias, with an overwhelming majority of cases of drug-induced LQTS stemming from impaired hERG channel function (Roden, 2004). hERG channel function, conducting a crucial repolarizing current in the heart, can be inhibited either by acute blockade or by decreasing channel density at the membrane surface (Dennis et al., 2012; Ficker et al., 2004; Guo et al., 2007; Mitcheson et al., 2000a; Rajamani et al., 2006; Wang et al., 2007). Results presented in this study provide evidence for a distinctly novel mechanism of  $I_{hERG}$  modulation. For the first time, we show that the persistent inhibition of the hERG channel by AMIO reduces  $I_{hERG}$  without any effect on mature channel expression. More specifically, despite the two-time washes with D-PBS and voltage-clamp recordings performed in a drug-free bath solution, overnight culture with the drug irreversibly abolished  $I_{hERG}$  but did not affect surface channel expression (Figs. 6 and 7). However, similar to agents that do reduce mature hERG expression, recovery of  $I_{hERG}$  from AMIO-mediated inhibition depended solely on the forward trafficking of newly made channels to the membrane surface (Fig. 11). (Rajamani et al., 2006).

DEA, the major active metabolite of AMIO, is also known to block hERG channel conductance. While less potent than its parent compound, DEA still irreversibly blocks  $I_{hERG}$  with an  $IC_{50}$  of  $0.95 \mu\text{M}$  and, like AMIO, does not affect mature channel expression (Fig. 13). Therefore, we hypothesize that DEA may also modulate the rate of mature channel degradation, although further experiments are required to confirm this. In this case, cells with DEA-blocked channels would also rely on forward trafficking of newly made channels to recover  $I_{hERG}$ .

To probe the electrophysiological effects of the AMIO-hERG interaction, we used whole-cell voltage-clamp recordings. Here, we showed that AMIO binding to the channel occurs

predominantly in its open and/or inactivated states and channel block develops faster at shorter pulse intervals, confirming AMIO as a use- and frequency-dependent hERG channel blocker (Fig. 9). We also provided the first evidence for a persistent  $I_{\text{hERG}}$  inhibition, despite thorough washout of the drug prior to electrophysiological recordings (Fig. 8). When studying the structural components of the hERG channel that facilitate such strong drug interaction, our mutagenesis results indicated strong binding affinity for the common drug-binding sites located on the S6 domain, namely Y652 and F656 (Fig. 10). These aromatic residues project into the pore cavity and have been widely described as responsible for most cases of drug-induced hERG blockade and thus LQTS (Mitcheson et al., 2000a). Furthermore, only the S620T inactivation-deficient mutant, unlike S631A, showed a significant increase in the  $IC_{50}$  value of AMIO-induced block (Fig. 10). These have been found to attenuate drug binding by removing hERG inactivation kinetics and preventing the rearrangement within the SF that orients residues Y652 and F656 towards the ion conduction pathway (Butler et al., 2019). Considering the location of either of these residues – S620 inside and S631 outside the pore mouth – these results further support our previous evidence for high-affinity binding to Y652 and F656. These data point to ‘drug trapping’ as one potential mechanism responsible for the observed irreversible channel block, whereby the drug becomes ‘trapped’ within the pore cavity by the closure of the activation gate (Mitcheson et al., 2000b). Finally, the binding affinity of AMIO towards the hERG channel remained unaffected by the  $\Delta$ 2-354 and  $\Delta$ C-1073 mutants (Fig. 10). While these results provide valuable information on the residues involved in the AMIO-hERG interaction, none of the above mutations removed the irreversible component of the AMIO-induced block (data not shown). Therefore, the persistent loss of hERG channel function induced by AMIO binding remains unexplained from the mechanistic standpoint. In addition, whether AMIO-induced inhibition of other ion channels expressed in

native cardiac cells is also irreversible remains unknown, as this study was focused solely on the drug's interaction with the hERG channel.

Due to the high lipophilicity of AMIO, it is possible that the plasma membrane may have acted as a reservoir for the drug, slowly releasing it to prolong the channel-blocking effects and creating a functional equivalent of the persistent block observed in this study (Vauquelin, 2016). While this is a plausible mechanism, our experimental results indicate otherwise. As can be seen in Fig. 11C,  $I_{hERG}$  stayed inhibited in AMIO-pretreated cells for the duration of the 4-hour culture with BFA+Baf while the upper band – representing mature channels – slowly decayed. On the other hand, 4-hour-long recovery following PK cleavage of surface channels pretreated with AMIO resulted in the gradual return of both the upper band and a substantial  $I_{hERG}$  conductance. Since the newly made channels were fully functional in the AMIO-pretreated PK-treated cells, this mechanism did not appear to contribute to the persistent inhibitory effect on  $I_{hERG}$ . In other words, if the plasma membrane were in fact to serve as a reservoir for AMIO, newly made channels would also become blocked by the residual drug within the membrane, thus rendering the aforementioned theory irrelevant. Furthermore, our experimental results showed increased susceptibility of AMIO-pretreated mature hERG channels to internalization and subsequent degradation (Fig. 12A). Taken together, these data further support the idea of a permanent AMIO-hERG interaction, independent of the membrane AMIO content, that forces the channels to undergo an irreversible loss of function, likely due to a conformational change, making them a target for accelerated degradation.

Conformational changes within mature hERG channels, such as those observed in the absence of extracellular  $K^+$ , have been described to accelerate internalization of the channels (Guo et al., 2009; Guo et al., 2011; Massaeli et al., 2010). This has been attributed to the exposure of internalization signals resulting from the conformational change and causing a reduction in surface

density of the channels and impaired outward  $K^+$  conductance (AlRawashdeh et al., 2024). However, the prevention or reversal of this conformational change, for example by interactions with other membrane proteins, have been shown to enhance membrane stability of the mature hERG channels (Guo et al., 2011). The increased rate of internalization of amiodarone-blocked hERG channels (Fig. 12A) appears to contradict our results showing no effect on mature channel expression following overnight exposure to various concentrations of AMIO (Fig. 7A). However, when AMIO was left in the culture medium alongside BFA in AMIO-pretreated cells, the rate of degradation slowed (Fig. 12A). While the mechanism underlying this phenomenon is not yet known, we propose that the hERG protein may possess two distinct binding sites for AMIO. Binding to the first site occurs with higher affinity, is irreversible, and causes a persistent conformational change within the protein that translates to a resulting loss of  $I_{hERG}$  conductance and enhanced degradation. Interaction with the second binding site then stabilizes the channels at the membrane surface, likely by reversing the conformational change and thus the enhanced degradation. Binding at this site is reversible, explaining the faster degradation of mature hERG protein in AMIO-pretreated cells further cultured in the absence of the drug. So far, this AMIO-mediated reversal of accelerated mature channel degradation but not current inhibition remains unexplained.

In terms of clinical significance, the irreversible inhibition of hERG channel function by AMIO and DEA could explain their long-lasting therapeutic effects. Elimination kinetics of AMIO are extremely slow, and its plasma concentration remains within the therapeutic range for over a month (Kannan et al., 1987; Latini et al., 1984; Marchiset et al., 1985; Zhang et al., 2010). While a wide range plasma concentrations have been reported for AMIO and DEA (0.5-2.8  $\mu\text{g}/\text{ml}$  and 0.8-2.2  $\mu\text{g}/\text{ml}$ , respectively), the majority of both compounds remain protein-bound, with less than

0.01% of AMIO existing in its free unbound form available to exert its antiarrhythmic effects (Heger et al., 1984; Pollak et al., 2000; Veronese et al., 1988). Due to this high variation, QT interval prolongation has been found to be a more valuable tool for assessing arrhythmogenic risk (Kannan et al., 1987; Markos et al., 1985; Torres et al., 1986). Combined with the extended effects of DEA, this presents a significant clinical concern following therapy discontinuation due to an episode of TdP, as both compounds' therapeutic effects take a long time to decline (Drew et al., 2010; Kannan et al., 1987; Latini et al., 1984; Marchiset et al., 1985; Thomas and Behr, 2016). Considering the lack of an antagonistic therapy for AMIO- and DEA-induced TdP and the novel information added by this study on the persistent blockade of the hERG channel by both compounds, patients' recovery period would require until functional channels are produced and trafficked to the membranes of ventricular cardiomyocytes to restore the repolarizing capacity of the ventricular tissue. This is in stark contrast to other class III antiarrhythmics, where  $I_{hERG}$  recovers rapidly upon drug washout. Therefore, prolonged electrophysiological monitoring of patients undergoing withdrawal of AMIO therapy is paramount to ensure minimal risk of recurrent episodes of TdP.

### **Future directions**

This study is not without its limitations. First, all of the experiments conducted in this study utilized cell lines expressing exclusively the hERG 1a isoform. It has been shown in literature that heterotetrameric hERG channels resulting from the assembly of hERG 1a- and 1b-encoded subunits exhibit different affinity for drug interactions when compared to homotetrameric hERG 1a channels (Abi-Gerges et al., 2011). Therefore, inducing expression of both the 1a and 1b isoforms would provide a more realistic idea of the  $I_{hERG}$ -inhibitory effects of both AMIO and DEA. However, we expect that while the altered gating kinetics of heterotetrameric hERG

channels may have an effect on both compounds' overall binding affinity, the identical pore-forming regions shared between 1a and 1b isoforms would likely preclude the washout of either AMIO or DEA (Sale et al., 2008). Second, we did not use tissue samples natively expressing hERG channel subunits. Instead, we used an immortalized rat cardiomyocyte-derived H9c2 cell line transiently transfected with WT hERG cDNA to provide a representation of primary cardiomyocytes for the purposes of this study. However, our results need to be further verified using a model natively expressing both the 1a and 1b isoforms of the ERG channels with a physiologically-relevant ratio of the two, as this was also found to affect  $I_{Kr}$  kinetics (McNally et al., 2017). Finally, while this study did investigate DEA-mediated inhibition of  $I_{hERG}$  as well as its washout properties, effects on the rate of mature channel degradation were not directly probed, thus further experiments are required.

When it comes to future research avenues presented by this study, the exact mechanism of AMIO- and DEA-induced inhibition of mature hERG channels remains a principal question. Mathematical docking models or cryo-electron microscopy techniques could shine a light on the precise nature of the AMIO-hERG interaction and possibly aid in the development of highly-effective antiarrhythmic drugs. In addition, the channel-stabilizing effect of AMIO in AMIO-pretreated cells certainly warrants further investigation. It would therefore be interesting to investigate whether AMIO can prevent the accelerated degradation of mature hERG channels, such as that caused by low extracellular  $K^+$ .

## References

- Abi-Gerges N, Holkham H, Jones EM, Pollard CE, Valentin JP and Robertson GA (2011) hERG subunit composition determines differential drug sensitivity. *Br J Pharmacol* **164**(2b): 419-432.
- Akhavan A, Atanasiu R and Shrier A (2003) Identification of a COOH-terminal segment involved in maturation and stability of human ether-a-go-go-related gene potassium channels. *J Biol Chem* **278**(41): 40105-40112.
- AlRawashdeh S, Mosa FES and Barakat KH (2024) Computational insights into the mechanisms underlying structural destabilization and recovery in trafficking-deficient hERG mutants. *Front Mol Biosci* **11**: 1341727.
- Amin AS, Tan HL and Wilde AA (2010) Cardiac ion channels in health and disease. *Heart Rhythm* **7**(1): 117-126.
- Bailie DS, Inoue H, Kaseda S, Ben-David J and Zipes DP (1988) Magnesium suppression of early afterdepolarizations and ventricular tachyarrhythmias induced by cesium in dogs. *Circulation* **77**(6): 1395-1402.
- Baruscotti M, Bucchi A and DiFrancesco D (2005) Physiology and pharmacology of the cardiac pacemaker ("funny") current. *Pharmacol Ther* **107**(1): 59-79.
- Behar J, Ganesan A, Zhang J and Yaniv Y (2016) The Autonomic Nervous System Regulates the Heart Rate through cAMP-PKA Dependent and Independent Coupled-Clock Pacemaker Cell Mechanisms. *Front Physiol* **7**: 419.
- Belardinelli L, Antzelevitch C and Vos MA (2003) Assessing predictors of drug-induced torsade de pointes. *Trends Pharmacol Sci* **24**(12): 619-625.

- Butler A, Helliwell MV, Zhang Y, Hancox JC and Dempsey CE (2019) An Update on the Structure of hERG. *Front Pharmacol* **10**: 1572.
- Chen J, Seeböhm G and Sanguinetti MC (2002) Position of aromatic residues in the S6 domain, not inactivation, dictates cisapride sensitivity of HERG and eag potassium channels. *Proc Natl Acad Sci U S A* **99**(19): 12461-12466.
- DeMarco KR and Clancy CE (2016) Cardiac Na Channels: Structure to Function. *Curr Top Membr* **78**: 287-311.
- Dennis AT, Wang L, Wan H, Nassal D, Deschenes I and Ficker E (2012) Molecular determinants of pentamidine-induced hERG trafficking inhibition. *Mol Pharmacol* **81**(2): 198-209.
- Dhamoon AS and Jalife J (2005) The inward rectifier current (IK1) controls cardiac excitability and is involved in arrhythmogenesis. *Heart Rhythm* **2**(3): 316-324.
- Drew BJ, Ackerman MJ, Funk M, Gibler WB, Kligfield P, Menon V, Philippides GJ, Roden DM, Zareba W, American Heart Association Acute Cardiac Care Committee of the Council on Clinical Cardiology tCoCN and the American College of Cardiology F (2010) Prevention of torsade de pointes in hospital settings: a scientific statement from the American Heart Association and the American College of Cardiology Foundation. *Circulation* **121**(8): 1047-1060.
- Drouin E, Lande G and Charpentier F (1998) Amiodarone reduces transmural heterogeneity of repolarization in the human heart. *J Am Coll Cardiol* **32**(4): 1063-1067.
- Ferrer T, Rupp J, Piper DR and Tristani-Firouzi M (2006) The S4-S5 linker directly couples voltage sensor movement to the activation gate in the human ether-a'-go-go-related gene (hERG) K<sup>+</sup> channel. *J Biol Chem* **281**(18): 12858-12864.

- Ficker E, Dennis AT, Wang L and Brown AM (2003) Role of the cytosolic chaperones Hsp70 and Hsp90 in maturation of the cardiac potassium channel HERG. *Circ Res* **92**(12): e87-100.
- Ficker E, Kuryshev YA, Dennis AT, Obejero-Paz C, Wang L, Hawryluk P, Wible BA and Brown AM (2004) Mechanisms of arsenic-induced prolongation of cardiac repolarization. *Mol Pharmacol* **66**(1): 33-44.
- Foo B, Barbier C, Guo K, Vasantharuban J, Lukacs GL and Shrier A (2019) Mutation-specific peripheral and ER quality control of hERG channel cell-surface expression. *Sci Rep* **9**(1): 6066.
- Foo B, Williamson B, Young JC, Lukacs G and Shrier A (2016) hERG quality control and the long QT syndrome. *J Physiol* **594**(9): 2469-2481.
- Freedman MD and Somberg JC (1991) Pharmacology and pharmacokinetics of amiodarone. *J Clin Pharmacol* **31**(11): 1061-1069.
- Gelman I, Sharma N, McKeeman O, Lee P, Campagna N, Tomei N, Baranchuk A, Zhang S and El-Diasty M (2024) The ion channel basis of pharmacological effects of amiodarone on myocardial electrophysiological properties, a comprehensive review. *Biomed Pharmacother* **174**: 116513.
- Ghovanloo MR, Abdelsayed M and Ruben PC (2016) Effects of Amiodarone and N-desethylamiodarone on Cardiac Voltage-Gated Sodium Channels. *Front Pharmacol* **7**: 39.
- Grant AO (2009) Cardiac ion channels. *Circ Arrhythm Electrophysiol* **2**(2): 185-194.
- Guo J, Massaeli H, Li W, Xu J, Luo T, Shaw J, Kirshenbaum LA and Zhang S (2007) Identification of IKr and its trafficking disruption induced by probucol in cultured neonatal rat cardiomyocytes. *J Pharmacol Exp Ther* **321**(3): 911-920.

- Guo J, Massaeli H, Xu J, Jia Z, Wigle JT, Mesaeli N and Zhang S (2009) Extracellular K<sup>+</sup> concentration controls cell surface density of IKr in rabbit hearts and of the HERG channel in human cell lines. *J Clin Invest* **119**(9): 2745-2757.
- Guo J, Wang T, Yang T, Xu J, Li W, Fridman MD, Fisher JT and Zhang S (2011) Interaction between the cardiac rapidly (IKr) and slowly (IKs) activating delayed rectifier potassium channels revealed by low K<sup>+</sup>-induced hERG endocytic degradation. *J Biol Chem* **286**(40): 34664-34674.
- Gupta A, Lawrence AT, Krishnan K, Kavinsky CJ and Trohman RG (2007) Current concepts in the mechanisms and management of drug-induced QT prolongation and torsade de pointes. *Am Heart J* **153**(6): 891-899.
- Gustina AS and Trudeau MC (2011) hERG potassium channel gating is mediated by N- and C-terminal region interactions. *J Gen Physiol* **137**(3): 315-325.
- Gustina AS and Trudeau MC (2012) HERG potassium channel regulation by the N-terminal eag domain. *Cell Signal* **24**(8): 1592-1598.
- Heger JJ, Solow EB, Prystowsky EN and Zipes DP (1984) Plasma and red blood cell concentrations of amiodarone during chronic therapy. *Am J Cardiol* **53**(7): 912-917.
- Helliwell MV, Zhang Y, El Harchi A, Dempsey CE and Hancox JC (2023) Inhibition of the hERG Potassium Channel by a Methanesulphonate-Free E-4031 Analogue. *Pharmaceuticals (Basel)* **16**(9).
- Horvath B, Banyasz T, Jian Z, Hegyi B, Kistamas K, Nanasi PP, Izu LT and Chen-Izu Y (2013) Dynamics of the late Na<sup>(+)</sup> current during cardiac action potential and its contribution to afterdepolarizations. *J Mol Cell Cardiol* **64**: 59-68.

- Horvath B, Hegyi B, Kistamas K, Vaczi K, Banyasz T, Magyar J, Szentandrassy N and Nanasi PP (2015) Cytosolic calcium changes affect the incidence of early afterdepolarizations in canine ventricular myocytes. *Can J Physiol Pharmacol* **93**(7): 527-534.
- Istratoaie S, Sabin O, Vesa Ş C, Cismaru G, Donca VI and Buzoianu AD (2021) Efficacy of amiodarone for the prevention of atrial fibrillation recurrence after cardioversion. *Cardiovasc J Afr* **32**(6): 327-338.
- Johnson AA, Crawford TR and Trudeau MC (2022) The N-linker region of hERG1a upregulates hERG1b potassium channels. *J Biol Chem* **298**(9): 102233.
- Jones DK, Liu F, Vaidyanathan R, Eckhardt LL, Trudeau MC and Robertson GA (2014) hERG 1b is critical for human cardiac repolarization. *Proc Natl Acad Sci U S A* **111**(50): 18073-18077.
- Kallergis EM, Goudis CA, Simantirakis EN, Kochiadakis GE and Vardas PE (2012) Mechanisms, risk factors, and management of acquired long QT syndrome: a comprehensive review. *ScientificWorldJournal* **2012**: 212178.
- Kalyaanamoorthy S and Barakat KH (2018) Binding modes of hERG blockers: an unsolved mystery in the drug design arena. *Expert Opin Drug Discov* **13**(3): 207-210.
- Kamiya K, Mitcheson JS, Yasui K, Kodama I and Sanguinetti MC (2001) Open channel block of HERG K(+) channels by vesnarinone. *Mol Pharmacol* **60**(2): 244-253.
- Kannan R, Yabek SM, Garson A, Jr., Miller S, McVey P and Singh BN (1987) Amiodarone efficacy in a young population: relationship to serum amiodarone and desethylamiodarone levels. *Am Heart J* **114**(2): 283-287.

- Kaseda S, Gilmour RF, Jr. and Zipes DP (1989) Depressant effect of magnesium on early afterdepolarizations and triggered activity induced by cesium, quinidine, and 4-aminopyridine in canine cardiac Purkinje fibers. *Am Heart J* **118**(3): 458-466.
- Kauthale RR, Dadarkar SS, Husain R, Karande VV and Gatne MM (2015) Assessment of temperature-induced hERG channel blockade variation by drugs. *J Appl Toxicol* **35**(7): 799-805.
- Kiehn J, Lacerda AE and Brown AM (1999a) Pathways of HERG inactivation. *Am J Physiol* **277**(1): H199-210.
- Kiehn J, Thomas D, Karle CA, Schols W and Kubler W (1999b) Inhibitory effects of the class III antiarrhythmic drug amiodarone on cloned HERG potassium channels. *Naunyn Schmiedebergs Arch Pharmacol* **359**(3): 212-219.
- Kodama I, Kamiya K and Toyama J (1997) Cellular electropharmacology of amiodarone. *Cardiovasc Res* **35**(1): 13-29.
- Laemmli UK (1970) Cleavage of structural proteins during the assembly of the head of bacteriophage T4. *Nature* **227**(5259): 680-685.
- Latini R, Tognoni G and Kates RE (1984) Clinical pharmacokinetics of amiodarone. *Clin Pharmacokinet* **9**(2): 136-156.
- Lees-Miller JP, Duan Y, Teng GQ and Duff HJ (2000) Molecular determinant of high-affinity dofetilide binding to HERG1 expressed in *Xenopus* oocytes: involvement of S6 sites. *Mol Pharmacol* **57**(2): 367-374.
- Lefevre F, Remy MH and Masson JM (1997) Alanine-stretch scanning mutagenesis: a simple and efficient method to probe protein structure and function. *Nucleic Acids Res* **25**(2): 447-448.

- Li J, Shen R, Reddy B, Perozo E and Roux B (2021) Mechanism of C-type inactivation in the hERG potassium channel. *Sci Adv* **7**(5).
- Mantri N, Lu M, Zaroff JG, Risch N, Hoffmann T, Oni-Orisan A, Lee C and Iribarren C (2022) Torsade de pointes: A nested case-control study in an integrated healthcare delivery system. *Ann Noninvasive Electrocardiol* **27**(1): e12888.
- Marchiset D, Bruno R, Djiane P, Cano JP, Benichou M and Serradimigni A (1985) Amiodarone and desethylamiodarone elimination kinetics following withdrawal of long-term amiodarone maintenance therapy. *Biopharm Drug Dispos* **6**(2): 209-215.
- Markos J, Veronese ME, Nicholson MR, McLean S and Shevland JE (1985) Value of hepatic computerized tomographic scanning during amiodarone therapy. *Am J Cardiol* **56**(1): 89-92.
- Massaeli H, Guo J, Xu J and Zhang S (2010) Extracellular K<sup>+</sup> is a prerequisite for the function and plasma membrane stability of HERG channels. *Circ Res* **106**(6): 1072-1082.
- McNally BA, Pendon ZD and Trudeau MC (2017) hERG1a and hERG1b potassium channel subunits directly interact and preferentially form heteromeric channels. *J Biol Chem* **292**(52): 21548-21557.
- McPate MJ, Duncan RS, Hancox JC and Witchel HJ (2008) Pharmacology of the short QT syndrome N588K-hERG K<sup>+</sup> channel mutation: differential impact on selected class I and class III antiarrhythmic drugs. *Br J Pharmacol* **155**(6): 957-966.
- Milberg P, Ramtin S, Mönnig G, Osada N, Wasmer K, Breithardt G, Haverkamp W and Eckardt L (2004) Comparison of the in vitro electrophysiologic and proarrhythmic effects of amiodarone and sotalol in a rabbit model of acute atrioventricular block. *J Cardiovasc Pharmacol* **44**(3): 278-286.

- Milnes JT, Crociani O, Arcangeli A, Hancox JC and Witchel HJ (2003) Blockade of HERG potassium currents by fluvoxamine: incomplete attenuation by S6 mutations at F656 or Y652. *Br J Pharmacol* **139**(5): 887-898.
- Mitcheson JS, Chen J, Lin M, Culberson C and Sanguinetti MC (2000a) A structural basis for drug-induced long QT syndrome. *Proc Natl Acad Sci U S A* **97**(22): 12329-12333.
- Mitcheson JS, Chen J and Sanguinetti MC (2000b) Trapping of a methanesulfonanilide by closure of the HERG potassium channel activation gate. *J Gen Physiol* **115**(3): 229-240.
- Morais Cabral JH, Lee A, Cohen SL, Chait BT, Li M and Mackinnon R (1998) Crystal structure and functional analysis of the HERG potassium channel N terminus: a eukaryotic PAS domain. *Cell* **95**(5): 649-655.
- Mujovic N, Dobrev D, Marinkovic M, Russo V and Potpara TS (2020) The role of amiodarone in contemporary management of complex cardiac arrhythmias. *Pharmacol Res* **151**: 104521.
- Muskett FW, Thouta S, Thomson SJ, Bowen A, Stansfeld PJ and Mitcheson JS (2011) Mechanistic insight into human ether-à-go-go-related gene (hERG) K<sup>+</sup> channel deactivation gating from the solution structure of the EAG domain. *J Biol Chem* **286**(8): 6184-6191.
- Ng CA, Hunter MJ, Perry MD, Mobli M, Ke Y, Kuchel PW, King GF, Stock D and Vandenberg JJ (2011) The N-terminal tail of hERG contains an amphipathic alpha-helix that regulates channel deactivation. *PLoS One* **6**(1): e16191.
- Patel SP and Campbell DL (2005) Transient outward potassium current, 'I<sub>to</sub>', phenotypes in the mammalian left ventricle: underlying molecular, cellular and biophysical mechanisms. *J Physiol* **569**(Pt 1): 7-39.
- Perry M, Sanguinetti M and Mitcheson J (2010) Revealing the structural basis of action of hERG potassium channel activators and blockers. *J Physiol* **588**(Pt 17): 3157-3167.

- Perry MD, Ng CA, Mann SA, Sadrieh A, Imtiaz M, Hill AP and Vandenberg JI (2015) Getting to the heart of hERG K(+) channel gating. *J Physiol* **593**(12): 2575-2585.
- Pollak PT, Bouillon T and Shafer SL (2000) Population pharmacokinetics of long-term oral amiodarone therapy. *Clin Pharmacol Ther* **67**(6): 642-652.
- Rajamani S, Eckhardt LL, Valdivia CR, Klemens CA, Gillman BM, Anderson CL, Holzem KM, Delisle BP, Anson BD, Makielski JC and January CT (2006) Drug-induced long QT syndrome: hERG K<sup>+</sup> channel block and disruption of protein trafficking by fluoxetine and norfluoxetine. *Br J Pharmacol* **149**(5): 481-489.
- Ridley JM, Milnes JT, Witchel HJ and Hancox JC (2004) High affinity HERG K(+) channel blockade by the antiarrhythmic agent dronedarone: resistance to mutations of the S6 residues Y652 and F656. *Biochem Biophys Res Commun* **325**(3): 883-891.
- Roden DM (2004) Drug-induced prolongation of the QT interval. *N Engl J Med* **350**(10): 1013-1022.
- Sale H, Wang J, O'Hara TJ, Tester DJ, Phartiyal P, He JQ, Rudy Y, Ackerman MJ and Robertson GA (2008) Physiological properties of hERG 1a/1b heteromeric currents and a hERG 1b-specific mutation associated with Long-QT syndrome. *Circ Res* **103**(7): e81-95.
- Sanchez-Chapula JA, Ferrer T, Navarro-Polanco RA and Sanguinetti MC (2003) Voltage-dependent profile of human ether-a-go-go-related gene channel block is influenced by a single residue in the S6 transmembrane domain. *Mol Pharmacol* **63**(5): 1051-1058.
- Sanchez-Chapula JA, Navarro-Polanco RA, Culberson C, Chen J and Sanguinetti MC (2002) Molecular determinants of voltage-dependent human ether-a-go-go related gene (HERG) K<sup>+</sup> channel block. *J Biol Chem* **277**(26): 23587-23595.

- Sanguinetti MC, Jiang C, Curran ME and Keating MT (1995) A mechanistic link between an inherited and an acquired cardiac arrhythmia: HERG encodes the IKr potassium channel. *Cell* **81**(2): 299-307.
- Shan M, Jiang C, Qin L-P and Cheng G (2022) A Review of Computational Methods in Predicting hERG Channel Blockers. *ChemistrySelect* **7**(31): e202201221.
- Shayeganpour A, El-Kadi AO and Brocks DR (2006) Determination of the enzyme(s) involved in the metabolism of amiodarone in liver and intestine of rat: the contribution of cytochrome P450 3A isoforms. *Drug Metab Dispos* **34**(1): 43-50.
- Shi YP, Thouta S and Claydon TW (2020) Modulation of hERG K(+) Channel Deactivation by Voltage Sensor Relaxation. *Front Pharmacol* **11**: 139.
- Sicouri S and Antzelevitch C (1991) A subpopulation of cells with unique electrophysiological properties in the deep subepicardium of the canine ventricle. The M cell. *Circ Res* **68**(6): 1729-1741.
- Sicouri S, Moro S, Litovsky S, Elizari MV and Antzelevitch C (1997) Chronic amiodarone reduces transmural dispersion of repolarization in the canine heart. *J Cardiovasc Electrophysiol* **8**(11): 1269-1279.
- Smith PL, Baukrowitz T and Yellen G (1996) The inward rectification mechanism of the HERG cardiac potassium channel. *Nature* **379**(6568): 833-836.
- Sobie EA and Ramay HR (2009) Excitation-contraction coupling gain in ventricular myocytes: insights from a parsimonious model. *J Physiol* **587**(Pt 6): 1293-1299.
- Thomas SH and Behr ER (2016) Pharmacological treatment of acquired QT prolongation and torsades de pointes. *Br J Clin Pharmacol* **81**(3): 420-427.

- Torres V, Tepper D, Flowers D, Wynn J, Lam S, Keefe D, Miura DS and Somberg JC (1986) QT prolongation and the antiarrhythmic efficacy of amiodarone. *J Am Coll Cardiol* **7**(1): 142-147.
- Tristani-Firouzi M, Chen J, Mitcheson JS and Sanguinetti MC (2001) Molecular biology of K(+) channels and their role in cardiac arrhythmias. *Am J Med* **110**(1): 50-59.
- Tsuji Y, Yamazaki M, Shimojo M, Yanagisawa S, Inden Y and Murohara T (2024) Mechanisms of torsades de pointes: an update. *Front Cardiovasc Med* **11**: 1363848.
- Tsumoto K and Kurata Y (2022) Bifurcations and Proarrhythmic Behaviors in Cardiac Electrical Excitations. *Biomolecules* **12**(3).
- Van Herendael H and Dorian P (2010) Amiodarone for the treatment and prevention of ventricular fibrillation and ventricular tachycardia. *Vasc Health Risk Manag* **6**: 465-472.
- Vandenberg JI, Perozo E and Allen TW (2017) Towards a Structural View of Drug Binding to hERG K(+) Channels. *Trends Pharmacol Sci* **38**(10): 899-907.
- Vandenberg JI, Varghese A, Lu Y, Bursill JA, Mahaut-Smith MP and Huang CL (2006) Temperature dependence of human ether-a-go-go-related gene K<sup>+</sup> currents. *Am J Physiol Cell Physiol* **291**(1): C165-175.
- Vauquelin G (2016) Cell membranes... and how long drugs may exert beneficial pharmacological activity in vivo. *Br J Clin Pharmacol* **82**(3): 673-682.
- Veronese ME, McLean S and Hendriks R (1988) Plasma protein binding of amiodarone in a patient population: measurement by erythrocyte partitioning and a novel glass-binding method. *Br J Clin Pharmacol* **26**(6): 721-731.

- Wagner JA, Weisman HF, Levine JH, Snowman AM and Snyder SH (1990) Differential effects of amiodarone and desethylamiodarone on calcium antagonist receptors. *J Cardiovasc Pharmacol* **15**(3): 501-507.
- Wang L, Wible BA, Wan X and Ficker E (2007) Cardiac glycosides as novel inhibitors of human ether-a-go-go-related gene channel trafficking. *J Pharmacol Exp Ther* **320**(2): 525-534.
- White CM, Xie J, Chow MS and Kluger J (1999) Prophylactic magnesium to decrease the arrhythmogenic potential of class III antiarrhythmic agents in a rabbit model. *Pharmacotherapy* **19**(5): 635-640.
- Wolfes J, Sörgel R, Ellermann C, Frommeyer G and Eckardt L (2024) Mechanisms underlying the spontaneous termination of torsades de pointes in an experimental model of long QT syndrome. *Heart Rhythm*.
- Wood SA, Park JE and Brown WJ (1991) Brefeldin A causes a microtubule-mediated fusion of the trans-Golgi network and early endosomes. *Cell* **67**(3): 591-600.
- Yonai R, Kawabata M, Maeda S, Kawashima T, Tsuda Y, Nakasone T, Nakane H and Hirao K (2021) Torsade de pointes induced by intravenous amiodarone therapy accompanied by marked augmentation of the transmural dispersion of repolarization in a patient with tachycardia-induced-cardiomyopathy. *Ann Noninvasive Electrocardiol* **26**(3): e12810.
- Zhang S, Zhou Z, Gong Q, Makielski JC and January CT (1999) Mechanism of block and identification of the verapamil binding domain to HERG potassium channels. *Circ Res* **84**(9): 989-998.
- Zhang Y, Colenso CK, El Harchi A, Cheng H, Witchel HJ, Dempsey CE and Hancox JC (2016) Interactions between amiodarone and the hERG potassium channel pore determined with mutagenesis and in silico docking. *Biochem Pharmacol* **113**: 24-35.

Zhang YH, Cheng H, Alexeenko VA, Dempsey CE and Hancox JC (2010) Characterization of recombinant hERG K(+) channel inhibition by the active metabolite of amiodarone desethyl-amiodarone. *J Electrocardiol* **43**(5): 440-448.

Zou A, Xu QP and Sanguinetti MC (1998) A mutation in the pore region of HERG K<sup>+</sup> channels expressed in *Xenopus* oocytes reduces rectification by shifting the voltage dependence of inactivation. *J Physiol* **509** ( Pt 1)(Pt 1): 129-137.

Zünkler BJ (2006) Human ether-a-go-go-related (HERG) gene and ATP-sensitive potassium channels as targets for adverse drug effects. *Pharmacol Ther* **112**(1): 12-37.